Real-Time Multiple Fluid Simulation and Rendering on GPUs

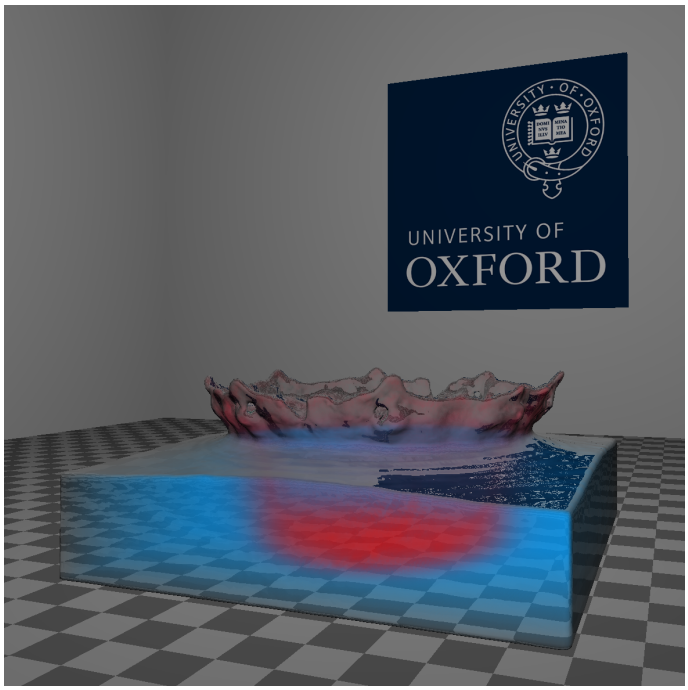

Candidate Number: 1023011

University of Oxford

Computer Science 3rd Year Project Report

Supervised by: Joe Pitt-Francis

Trinity 2020

Abstract

Fluid simulation is an extremely common and important computational task. These simulations are often heavily expensive and require a large amount of CPU time, and are hence difficult to apply in real-time applications. Fortunately, modern GPUs, equipped with massively parallel general-purpose computing architectures, provide a solution to this problem. This project explores methods to perform fluid simulations on GPUs, and to realistically render the simulated fluids, both in real time.

This project focuses on the fluid simulation algorithm known as FLIP (Fluid-Implicit-Particle), which is widely used in the computer graphics industry. The project studies how the algorithm can be parallelized, and creates an efficient GPU implementation using the CUDA programming model released by NVIDIA Cooperation. This project also extends the FLIP algorithm to support multiphase fluid simulation, thereby capturing the diffusion phenomenon between different fluids of different colours and densities. Alongside the simulation, a real-time liquid rendering scheme is implemented, which includes a novel algorithm for rendering the varying concentrations of coloured fluids inside the volume of liquid. A program that integrates all of these algorithms was created, which accepts user-provided simulation parameters, and performs the simulation in real time while rendering and displaying realistic animations.

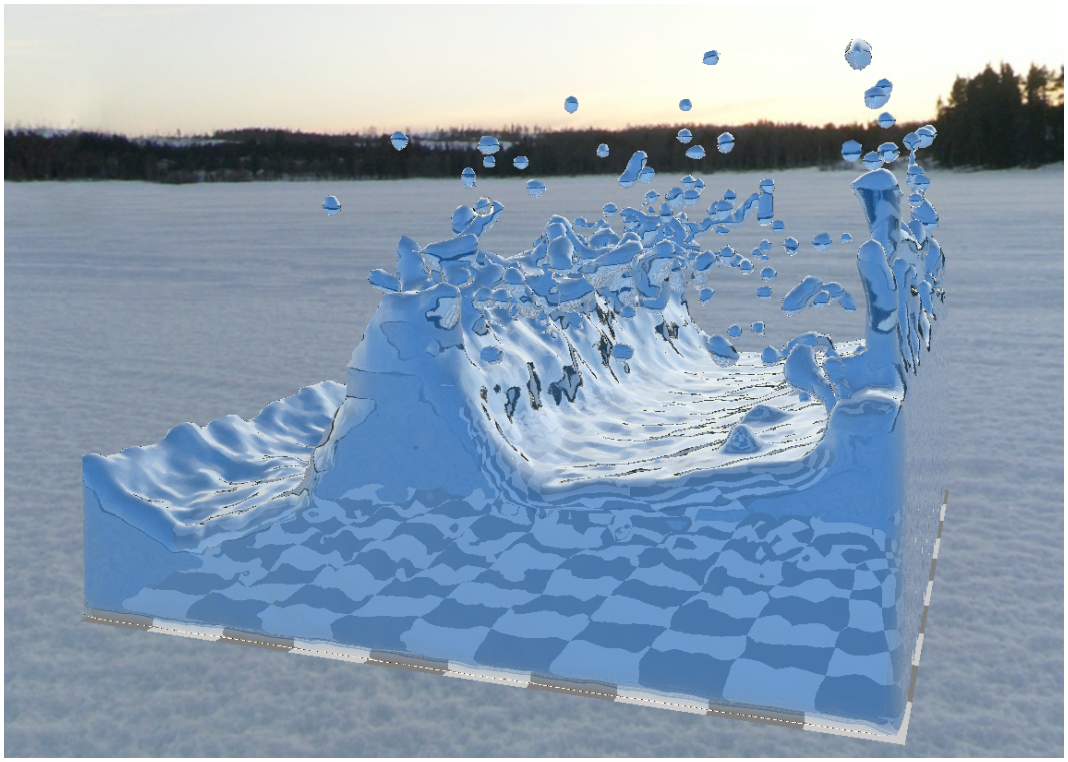

(a) A water simulation

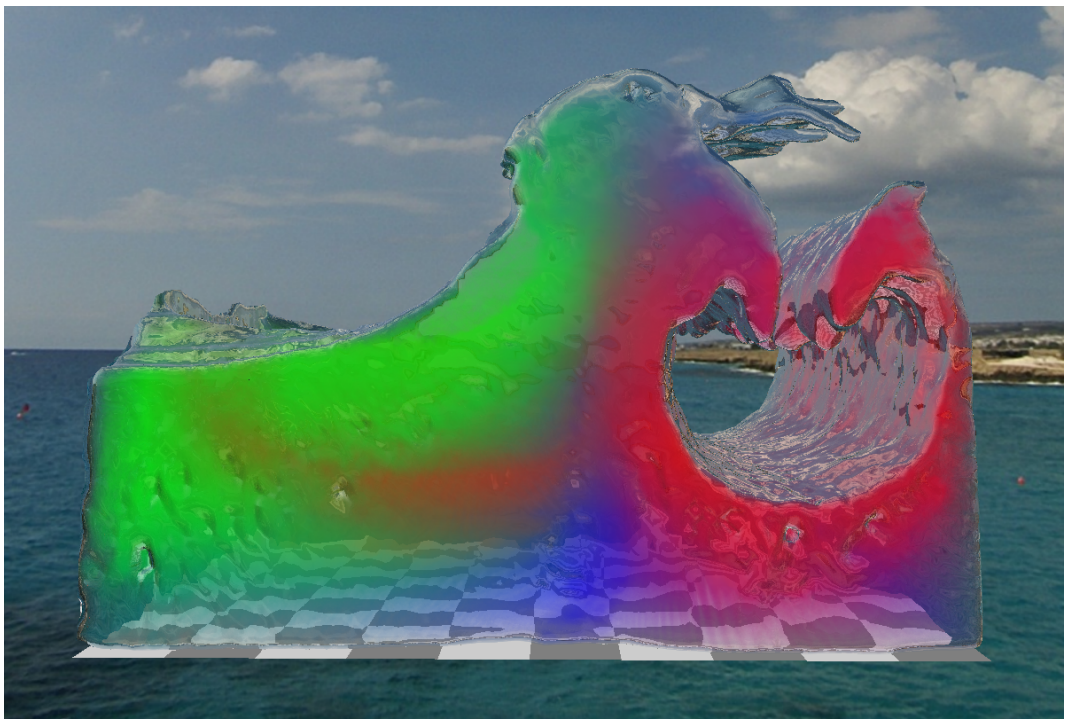

(b) A multi-fluid simulation

Figure 1: Screenshots of the fluid simulated and rendered by the software created in this project. More images can be found at `https://github.com/AmesingFlank/Aquarius`

Contents

1 Introduction

1.1 Motivation

Fluids can be seen everywhere. The smoke rising from the chimney and spreading in the wind, the milk in a cup mixing with the coffee, the calm flow of a river with tiny ripples under the rain, and the violent waves of the ocean shooting up and splashing down. Many of these phenomena have stunning visual effects, and quite often, realistic images of these fluids need to be computationally generated for purposes such as cinematics and video games.

Due to the mathematical complexity underlying the motion of fluids, accurate numerical simulations often require a vast amount of computation time. However, real-time computer graphics applications, such as video games, usually require the simulation to be computed in approximately the same amount of time as the physical process it represents. Moreover, in these applications, it is often required that the results of the simulation (i.e, the shape and motion of the fluid) are realistically rendered and displayed to the user. This project studies how these demands can be met on modern machines: by utilizing the parallel computing abilities of GPUs.

1.2 Related Work

The study of the behavior of fluids dates back to 18th century, when Leonhard Euler proposed a set of partial differential equations (PDEs), known as *Euler Equations*, that govern the behavior of an idealized incompressible and inviscid fluid. In the 19th century, these equations were extended by Claude-Louis Navier and George Gabriel Stokes into the famous *Navier-Stokes Equations*, which describe a much broader class of fluids that occur in the real world. These equations are explained in greater detail in chapter 2, and they are exactly what most fluid simulation software, including the one implemented in this project, are trying to solve.

Somewhat unfortunately, the Euler and Navier-Stokes equations have extremely difficult mathematical properties, and general analytical solutions are yet to be found

even today. As a result, fluid simulation software resort to numerical methods to approximate solutions. In computer graphics applications, there are two prominent families of numerical methods for solving the fluid equations: the grid-based methods and the particle-based methods. Each approach comes with its own benefits and drawbacks, but could both be implemented efficiently on GPUs to achieve real-time simulation.

The grid-based methods rely on spatial discretizations of the scalar and vector fields that represent the fluids. The most widely used discretization method, the **MAC** (Marker and Cell) **grid**, was proposed by Harlow and Welch[6] in 1965. Known for its high accuracy, this discretization scheme is the basis of most grid-based fluid simulation algorithms.

A significantly important step during a grid-based simulation is to move all the physical quantities stored in the grid (e.g. concentration) according to the velocity field. This step, known as *advection*, essentially determines how the shape of the fluid evolves over time. Thus, it is key to a high-fidelity simulation. A few popular advection algorithms include **MacCormack**[15] and **BFECC**[8], both of which have efficient GPU implementations[4][19]. This project chooses to implement the advection algorithm known as **FLIP** (Fluid Implicit Particle)[20], developed by Zhu and Bridson. This algorithm, interestingly enough, makes uses of particles to move quantities within the MAC grid. FLIP has various advantages over the purely grid-based algorithms, and is likely the most widely used advection method nowadays. The name FLIP consequently became a commonly used abbreviation for the full grid-based simulation with FLIP advection.

As an addition to the traditional single-phase fluid simulation, Kang[7] showed how to extend the grid-based algorithms to capture the diffusion between multiple miscible fluid phases (e.g. red ink spreading in transparent water). This project implements a modified version of the proposed algorithm, where FLIP, rather than BFECC, is used to advect the concentration of different fluid phases.

Apart from grid-based simulations, there is also a family of particle-based fluid simulation algorithms called **SPH** (Smoothed Particle Hydrodynamics), which does not rely on a grid. Originally developed for astronomical simulations by Lucy[10] and Monaghan[12] in 1977, SPH was introduced to computer graphics in 2003 by Müller[13]. The SPH method represents the fluid by a moving cloud of particles, which carry the physical quantities of the fluid with them. Two extensions of the SPH algorithm, namely PCISPH[16] and PBF[11], were studied and implemented in the early phases of this project. However, it was found that they could not match

the performance and accuracy of the FLIP algorithm. It was therefore decided that this project will focus mainly on FLIP.

On the rendering side, this project follows the proposal by Zhu and Bridson[20], who showed how a particle representation of a fluid could be used to compute a signed distance field, which represents the distance to the fluid surface of each point in the 3D space. An algorithm known as Marching Cubes, invented by Wyvill[18] and Lorensen[9], can then use this field to reconstruct the fluid's surface as a triangle mesh representation, which is suitable for rendering. Alternatively, screen-space algorithms[17] can be used, which do not generate a triangle mesh but directly uses the particles for rendering.

1.3 Project Outline

This project focuses on studying the FLIP fluid simulation algorithm and its GPU parallelization. The project extends the original FLIP, giving it the ability to simulate multiple fluids of different densities and colours, while capturing the diffusion phenomenon between them. In order to create an efficient GPU implementation of the algorithm, the project identifies parts of it that are not straightforwardly parallelizable, and overcomes these difficulties by investigating and implementing certain auxiliary parallel subroutines. Various memory access optimizations are also performed, so that the resulting implementation fully exploits the GPU's computation power and is fast enough to be used in real-time applications.

To visualize the simulations, the project implements a fast surface reconstruction algorithm, which transforms a particle cloud representation of fluids into a renderable triangle mesh. A real-time renderer is implemented to render the mesh while capturing all the reflection and refraction phenomena that occur in the real world. Furthermore, the renderer incorporates a novel algorithm that computes the different levels of attenuation of light caused by fluids of different colours, thereby also realistically rendering the liquid diffusion effects.

Integrating the simulation and rendering, the project creates a fully-featured program, which allows the user to easily set up a fluid simulation and obtain a rendered animation. The user can configure the shapes and sizes of the fluid before the simulation starts, as well as the initial colour and transparency of each fluid volume. The program can then carry out the simulation and render realistic results to the user in real time.

The software is developed for GPUs manufactured by the NVIDIA Cooperation, and utilizes NVIDIA's CUDA programming model. The OpenGL graphics API is used to interact with the GPU to render the fluid. The majority of the software consists of C++ code written for the CPU side of the program, and CUDA code for the GPU side. Additionally, a comparatively smaller amount of GLSL code is written specifically for rendering. With a total of over 13 thousand lines, the complete source code of the software can be found at `https://github.com/AmesingFlank/Aquarius`, along with some additional information and screenshots.

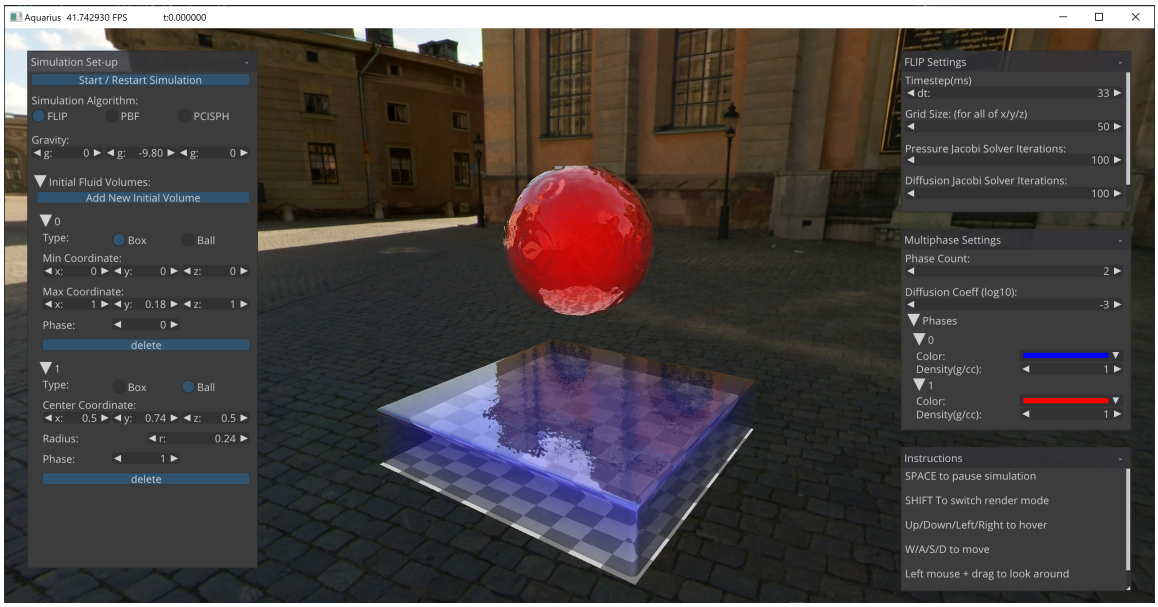

Figure 1.1: The full user interface of the software

2 Physics of Fluids

The mechanics of fluids are governed by the partial differential equations (PDEs) known as the *Incompressible Navier-Stokes Equations*, or in case of inviscid fluids, the *Euler Equations*. This chapter explains the meaning and intuition behind these equations, which are key to designing and implementing numerical simulation algorithms.

2.1 Vector Calculus

The fluid equations are commonly written in the language of vector calculus. A brief introduction of the main concepts and operators involved is given in this chapter.

Scalar Field

A *scalar field* on $\mathbb{R}^3$ is a mapping $\phi : \mathbb{R}^3 \to \mathbb{R}$ from 3D cartesian coordinates to scalar values. Example scalar fields include fluid density, or pressure, where a scalar value can be sampled in each point of the 3D space.

Vector Field

A *vector field* on $\mathbb{R}^3$ is a mapping $\phi : \mathbb{R}^3 \to \mathbb{R}^3$ from 3D cartesian coordinates to 3D vectors. A commonly seen vector field is the velocity field $\mathbf{u}$, which describes the direction and speed of the fluid's movement at each point in the 3D space

The grad

Given a scalar field $\phi : \mathbb{R}^3 \to \mathbb{R}$, the *gradient* or *grad* of the field is a vector field written as $\nabla\phi$, and it is defined by:

$$\nabla\phi = \begin{pmatrix} \dfrac{\partial\phi}{\partial x} \\ \dfrac{\partial\phi}{\partial y} \\ \dfrac{\partial\phi}{\partial z} \end{pmatrix}$$

The grad of a scalar quantity ϕ represents the rate of change of ϕ across each dimension. Moreover, $\nabla\phi$ computes the direction of movement that causes the greatest increase in ϕ.

The ∇ operator can also be extended to scalar fields of higher dimensions: let $\phi : \mathbb{R}^N \to \mathbb{R}$ be an N-dimensional scalar field, $\nabla\phi$ is then defined as:

$$\nabla\phi \begin{pmatrix} x_1 \\ x_2 \\ \vdots \\ x_N \end{pmatrix} = \begin{pmatrix} \dfrac{\partial\phi}{\partial x_1} \\ \dfrac{\partial\phi}{\partial x_2} \\ \vdots \\ \dfrac{\partial\phi}{\partial x_N} \end{pmatrix}$$

The div

Given a vector field $\mathbf{u} : \mathbb{R}^3 \to \mathbb{R}^3$, the *divergence* or *div* of the field is a scalar field written as $\nabla \cdot \mathbf{u}$, and it is defined by:

$$\nabla \cdot \mathbf{u} = \nabla \cdot \begin{pmatrix} \mathbf{u}_x \\ \mathbf{u}_y \\ \mathbf{u}_z \end{pmatrix} = \frac{\partial \mathbf{u}_x}{\partial x} + \frac{\partial \mathbf{u}_y}{\partial y} + \frac{\partial \mathbf{u}_z}{\partial z}$$

If $\mathbf{u}$ is the velocity field, then the scalar field $\nabla \cdot \mathbf{u}$ represents the speed at which the fluid is expanding or shrinking at each 3D location. Thus, a velocity field that satisfies $\nabla \cdot \mathbf{u} = 0$ would keep the fluid in constant volume, which is how most fluids behave in the real world.

The curl

Given a vector field $\mathbf{u} : \mathbb{R}^3 \to \mathbb{R}^3$, the *curl* of the field is a scalar field written as $\nabla \times \mathbf{u}$, and it is defined by:

$$\nabla \times \mathbf{u} = \nabla \times \begin{pmatrix} \mathbf{u}_x \\ \mathbf{u}_y \\ \mathbf{u}_z \end{pmatrix} = \begin{pmatrix} \dfrac{\partial \mathbf{u}_z}{\partial y} - \dfrac{\partial \mathbf{u}_y}{\partial z} \\ \dfrac{\partial \mathbf{u}_x}{\partial z} - \dfrac{\partial \mathbf{u}_z}{\partial x} \\ \dfrac{\partial \mathbf{u}_y}{\partial x} - \dfrac{\partial \mathbf{u}_x}{\partial y} \end{pmatrix}$$

Informally, the curl of the velocity field is a measure of the local rotation of the fluid. Though not directly used in the equations and algorithms presented in this project, it is at the heart of a different class of algorithms, called the vortex methods[1].

The Laplacian

The *Laplacian* operator, written $\nabla \cdot \nabla$, is defined to be the divergence of the gradient. For scalar field ϕ, it can be computed that:

$$\nabla \cdot \nabla \phi = \frac{\partial^2 \phi}{\partial x^2} + \frac{\partial^2 \phi}{\partial y^2} + \frac{\partial^2 \phi}{\partial z^2}$$

The Laplacian describes the difference between the average value of ϕ in the neighborhood of a certain point and the value of ϕ at that point. As defined, this operator takes a scalar field and returns a scalar field. However, The Laplacian is also often extended to be applied to vector fields, where

$$\nabla \cdot \nabla \mathbf{u} = \begin{pmatrix} \nabla \cdot \nabla \mathbf{u}_x \\ \nabla \cdot \nabla \mathbf{u}_y \\ \nabla \cdot \nabla \mathbf{u}_z \end{pmatrix}$$

2.2 The Eulerian and Lagrangian Viewpoints

For any physical quantity that represents some property of a fluid, the field of that quantity, either scalar or vector, could be constantly evolving as time passes. There are two different approaches to tracking this rate of change: the Eulerian viewpoint and the Lagrangian viewpoint.

The Eulerian viewpoint considers the time derivative of quantities at fixed locations in the 3D space. For a scalar field ϕ which varies through time, its *Eulerian derivative* is simply $\frac{\partial \phi}{\partial t}$. To be more precise, the Eulerian derivative $\frac{\partial \phi}{\partial t}$, evaluated at point $\mathbf{x}$, is the rate of change of ϕ of the fluid at the fixed position $\mathbf{x}$, despite the fact that the fluid could be in motion. This has the immediate consequence that the concept of Eulerian derivative fails to capture the fact that physical quantities are carried around (i.e advected) by the fluid.

The Lagrangian viewpoint, on the other hand, tracks the rates of changes of quantities as it moves along the velocity field $\mathbf{u}$. In this approach, for a scalar field ϕ, its derivative with respect to time is written as $\frac{D\phi}{Dt}$, and defined to be

$$\frac{D\phi}{Dt} = \frac{\partial \phi}{\partial t} + \nabla \phi \cdot \mathbf{u}$$

This derivative, known as the *Lagrangian derivative* or *material derivative*, can be justified by treating the fluid as a collection of infinitesimal particles, each carrying some quantities and moving along the velocity field. At time t, for each particle p

with position $\mathbf{x}$, the quantity of ϕ it carries is $\phi_p = \phi(t, \mathbf{x}(p))$. The derivative with respect to t of this term computes the rate of change of ϕ_p:

$$\begin{aligned}\frac{d}{dt}\phi_p &= \frac{d}{dt}\phi(t, \mathbf{x}(t)) \\ &= \frac{\partial \phi}{\partial t} + \nabla\phi \cdot \frac{d\mathbf{x}}{dt} \\ &= \frac{\partial \phi}{\partial t} + \nabla\phi \cdot \mathbf{u} \\ &= \frac{D\phi}{Dt}\end{aligned}$$

which is precisely the Lagrangian derivative.

When formalizing the Euler and Navier-Stokes equations, the Lagrangian derivative $\dfrac{D}{Dt}$ will be automatically extended to be applied to vector fields, where each component of the vector field is differentiated separately. This allows the term $\dfrac{D\mathbf{u}}{Dt}$ to be written, representing the acceleration of the infinitesimal fluid particles:

$$\frac{D\mathbf{u}}{Dt} = \frac{\partial \mathbf{u}}{\partial t} + \begin{pmatrix}\nabla \mathbf{u}_x \cdot \mathbf{u} \\ \nabla \mathbf{u}_y \cdot \mathbf{u} \\ \nabla \mathbf{u}_z \cdot \mathbf{u}\end{pmatrix} \tag{2.1}$$

2.3 The Euler and Navier-Stokes Equations

Using the previously defined notations, the Euler equations, which govern the motion of an incompressible and inviscid fluid, can be written as

$$\begin{cases} \dfrac{D\mathbf{u}}{Dt} = -\dfrac{\nabla p}{\rho} + \mathbf{g} \\ \nabla \cdot \mathbf{u} = 0 \end{cases} \qquad \text{(Euler Equations)}$$

where $\mathbf{u}$ is the velocity field, p is pressure, ρ is the fluid's density, and $\mathbf{g}$ the acceleration caused by an external force field (e.g. gravity).

A generalized version of these equations is the famous incompressible Navier-Stokes equations, in which a term that describes viscosity is added:

$$\begin{cases} \dfrac{D\mathbf{u}}{Dt} = -\dfrac{\nabla p}{\rho} + \mathbf{g} + \nu\nabla \cdot \nabla \mathbf{u} \\ \nabla \cdot \mathbf{u} = 0 \end{cases} \qquad \text{(Navier-Stokes Equations)}$$

where ν is the kinematic viscosity coefficient.

As described in the last section, the quantity $(\nabla \cdot \mathbf{u})$ represents the rate at which the fluid is expanding or shrinking. Fluids in the real world usually remain in constant

volume, unless in extreme conditions. This motivates the equation $\nabla \cdot \mathbf{u} = 0$, included in both Euler and Navier-Stokes.

Besides the incompressibility condition, both Euler and Navier-Stokes include another equation known as the momentum equation (which is in fact a set of equations, because the quantities are vectors). The momentum equation essentially specifies Newton's 2nd law: $\mathbf{a} = \dfrac{\mathbf{F}}{m}$, i.e. the acceleration is the force divided by the mass.

As previously explained, the quantity $\dfrac{D\mathbf{u}}{Dt}$ represents the acceleration of the infinitesimal fluid particles. Thus, to explain the momentum equations, it remains to demonstrate that the right-hand side correctly computes the force divided by the mass. Let the mass of the infinitesimal particle be m, and let the force be separated into the internal forces within the fluid F_{in} and the external forces F_{ext}:

$$\frac{D\mathbf{u}}{Dt} = \frac{F_{in} + F_{ext}}{m}$$

With $\mathbf{g}$ representing the acceleration caused by an external force field (e.g gravity), this can be rewritten as

$$\frac{D\mathbf{u}}{Dt} = \frac{F_{in}}{m} + \mathbf{g}$$

The internal forces within a fluid are caused by an imbalance in pressure. Specifically, if one side of an infinitesimal particle experiences greater pressure than the opposite side, then the particle will be pushed towards the low-pressure region. This justifies why the pressure forces are in the direction of $-\nabla p$, which computes the direction of fastest decrease of pressure. It can be shown that the actual pressure force exerted on the particle is the negative pressure gradient $-\nabla p$ multiplied by its volume V, which gives

$$\frac{D\mathbf{u}}{Dt} = -\frac{V\nabla p}{m} + \mathbf{g}$$

Using $\rho = \dfrac{m}{V}$, this becomes:

$$\frac{D\mathbf{u}}{Dt} = -\frac{\nabla p}{\rho} + \mathbf{g}$$

which is Euler's momentum equation. It is important to note that the justifications given in this section merely offers intuitions, and is far from a rigorous mathematical derivation, which would not fit into this report due to its complexity.

The Navier-Stokes momentum equation extends the Euler momentum equation by considering viscosity. In a viscous fluid, the velocity of a particle tends to diffuse into its surrounding particles, causing the velocity in the neighborhood to converge into its average. The difference between the average of $\mathbf{u}$ in the neighborhood and

the value of $\mathbf{u}$ of the particle is captured by the Laplacian of the velocity: $\nabla \cdot \nabla \mathbf{u}$, thus adding a positive multiple of this quantity creates a viscous effect:

$$\frac{D\mathbf{u}}{Dt} = -\frac{\nabla p}{\rho} + \mathbf{g} + \nu \nabla \cdot \nabla \mathbf{u}$$

where ν is a constant property, known as the kinematic viscosity of the fluid. For water, which is a rather inviscid fluid, this quantity is negligible, at least for rendering purposes. When simulating water, considering the effects of viscosity requires considerable extra computation, while bringing little improvements to the visual fidelity. As a result, this project chooses to only solve the Euler equations during simulation.

2.4 Boundary Conditions

For a fluid region that is not the entirety of $\mathbb{R}^3$, boundary conditions must be specified, which define the fluid's behaviour on the physical boundaries of the fluid region.

When simulating liquids, there are two types of boundary conditions: the solid boundaries and the free-surface boundaries. At a solid boundary, the condition is

$$\mathbf{u} \cdot \mathbf{n} = 0$$

where $\mathbf{n}$ is the normal of the solid surface. This condition ensures that the fluid cannot flow into a solid.

The second type of boundary is the free-surface boundary, which is the boundary between the liquids and some region of space that is not occupied by anything. In this case, that region of space will not exert any force, and therefore pressure, to the fluid, which motivates the condition

$$p = 0$$

This free surface-condition can also be applied to the boundary between liquid and air, which is because air is significantly lighter than liquid, and hence does not influence the motion of the liquid.

The liquid simulated in this project is contained within a cubic box. Moreover, it does not fill the box entirely and thus has a free surface. Thus, both types of boundary conditions must be considered during the simulation.

2.5 Multiple Fluids

Finally, this section introduces an equation that governs the concentration changes in a mixture of more than one type of miscible fluids, for example, ink and water. In physics, the different types of fluids are sometimes referred to as *phases*.

The concentration of different fluid phases will be represented using *volume fractions*. Specifically, for an infinitesimal fluid element at location $\mathbf{x}$ with volume $\mathbf{V}(\mathbf{x})$, and let the portion of this volume occupied by the ith fluids phase be $\mathbf{V}^i(\mathbf{x})$, then the concentration of the ith phase at $\mathbf{x}$ will be $\alpha^i(\mathbf{x}) = \dfrac{\mathbf{V}^i(\mathbf{x})}{\mathbf{V}(\mathbf{x})}$. Together, the α^i for all phases form a vector $\boldsymbol{\alpha}$, whose components are non-negative and sum up to 1.

The diffusion among multiple fluid phases is a result of the random Brownian motion of the fluid particles. However, it is possible to model this process from a macroscopic viewpoint, where an equation can be written that governs the expectation of how the concentrations change:

$$\frac{D\alpha^i}{Dt} = C\nabla \cdot \nabla\alpha^i \qquad \text{(Advection-Diffusion Equation)}$$

where C is the diffusion coefficient. Informally, if the concentration of a fluid region has a different concentration than its surroundings, this difference tends to "diffuse" into the neighborhood, and thus be reduced. This explains why the rate of change (Lagrangian derivation) of the concentration is proportional to its Laplacian.

3 The FLIP Algorithm

This chapter explains the principles of the **FLIP** (Fluid Implicit Particle) algorithm for fluid simulation, and how it is derived from the Euler equations. Additionally, section 3.6 explains how this project extends the original FLIP algorithm to model multiple fluids with different physical properties, and how different miscible fluids diffuse into each other.

3.1 Operator Splitting

A common way for numerically solving differential equations is the *operator splitting* approach. As a simple example, consider the simple differential equation:

$$\frac{dx}{dt} = f(x) + g(x) \quad \text{With initial condition } x(0) = x_0$$

To numerically solve this, decide on some small time step $\triangle t$, and let $x_{[n]}$ be the value of x at the nth time step. The goal is to find $x_{[n]}$ for increasing larger n. To do this, start with $x_{[0]} = x_0$ and consider the two differential equations:

$$\frac{dx}{dt} = f(x)$$
$$\frac{dx}{dt} = g(x)$$

Suppose there exists some good solutions (either analytical or numerical) for these two equations, then these solutions can be used to find a good solution for the original equation. Specifically, suppose $F_{f_0}(t)$ is a solution of $\dfrac{dx}{dt} = f(x)$ with initial condition $x(0) = f_0$, and $G_{g_0}(t)$ is a solution of $\dfrac{dx}{dt} = g(x)$ with initial condition $x(0) = g_0$, then, the original equation can be solved as

$$\widetilde{x} = F_{x_{[n]}}(\triangle t)$$
$$x_{[n+1]} = G_{\widetilde{x}}(\triangle t)$$

In essence, this approach splits the equation into a few more easily solved differential equations, and accumulates the solution of each over a small time step.

This same splitting approach can be applied to the Euler equations. To do so, the Euler momentum equation is first written in a form where the material derivative is expanded using equation (2.1):

$$\frac{\partial \mathbf{u}}{\partial t} = -\begin{pmatrix} \nabla \mathbf{u}_x \cdot \mathbf{u} \\ \nabla \mathbf{u}_y \cdot \mathbf{u} \\ \nabla \mathbf{u}_z \cdot \mathbf{u} \end{pmatrix} + \mathbf{g} - \frac{\nabla p}{\rho}$$

This then allows the equation, and therefore the simulation algorithm, to be split into three parts:

1. $$\frac{\partial \mathbf{u}}{\partial t} = -\begin{pmatrix} \nabla \mathbf{u}_x \cdot \mathbf{u} \\ \nabla \mathbf{u}_y \cdot \mathbf{u} \\ \nabla \mathbf{u}_z \cdot \mathbf{u} \end{pmatrix}$$

   Again using equation (2.1), this can be rewritten back into the material derivative form:

   $$\frac{D\mathbf{u}}{Dt} = 0$$

   Intuitively, solving this equation means to move the fluid according to its velocity field, in a way such that the velocity of each infinitesimal fluid partial remains unchanged. This is the step known as *advection*.

2. $$\frac{\partial \mathbf{u}}{\partial t} = \mathbf{g}$$

   Solving this equation is the process of exerting external forces (e.g gravity) on the fluid. The solid boundary conditions can also be enforced in this step.

3. $$\frac{\partial \mathbf{u}}{\partial t} = -\frac{\nabla p}{\rho}$$

   Since this is the last step of the splitting, it is essential to make sure that the results of solving this equation satisfy the incompressibility condition $\nabla \cdot \mathbf{u} = 0$. This amounts to finding a pressure field p such that, subtracting $\triangle t \frac{\nabla p}{\rho}$ from $\mathbf{u}$ makes the velocity have zero divergence. This step enforces the incompressibility of the fluid.

3.2 Discretization

The Euler equations involve two crucial quantities: the pressure scalar field p, and the velocity vector field $\mathbf{u}$. For a numerical simulation, discretized versions of both fields need to maintained. A straightforward choice, which is used for the pressure field, is to maintain a 3d grid, where each cubic grid cell stores the pressure value sampled at the centre of the cell. As an example, this figure shows the cell with location (x, y, z), and 3 of its neighbors:

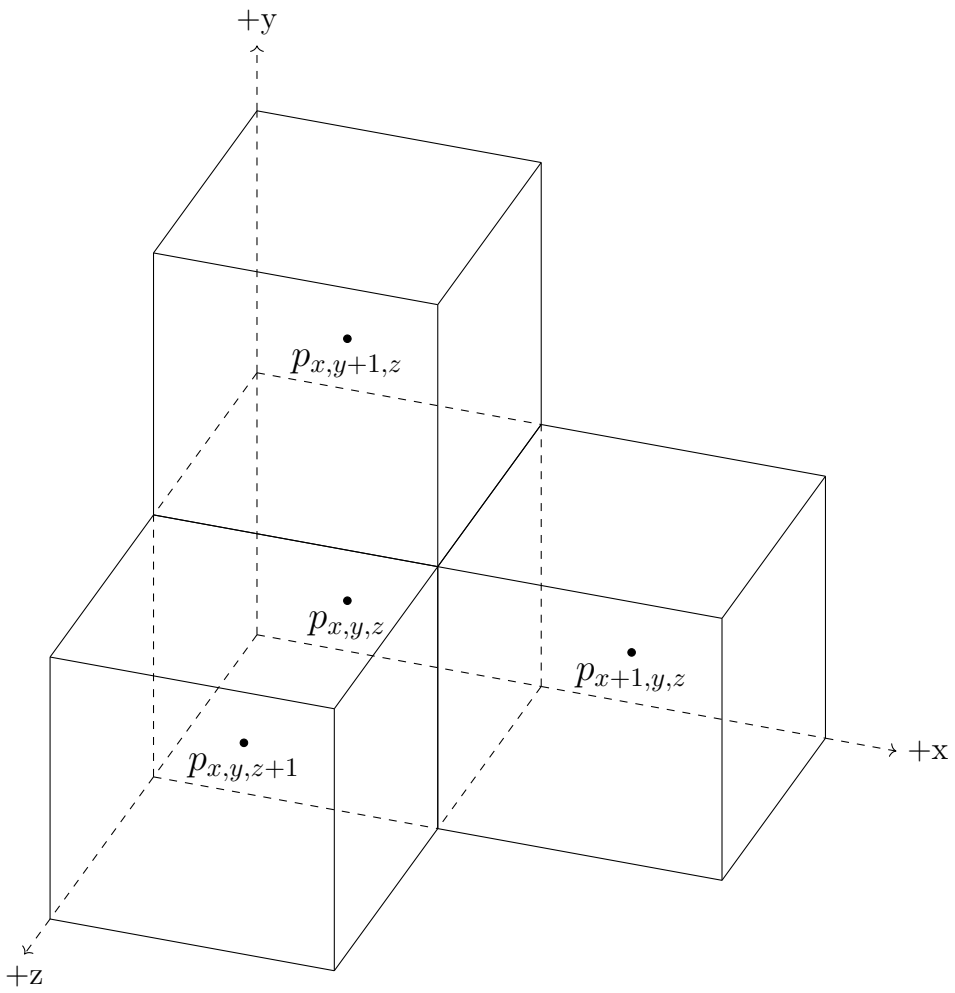

In this grid, p is only sampled at finitely many discrete locations, but it serves as an approximation of the continuous field. Specifically, the value $p(\mathbf{x})$ at a location $\mathbf{x}$ that is not a cell center can be approximated by interpolating nearby p samples.

Other than being simple to implement, this discretization scheme also has the advantage that the finite difference approximation of the Laplacian of the pressure field, sampled at the center of the cells, can be easily computed:

$$
\begin{aligned}
\nabla \cdot \nabla p &= \frac{\partial^2 p}{\partial x^2} + \frac{\partial^2 p}{\partial y^2} + \frac{\partial^2 p}{\partial z^2} \\
&\approx \frac{p_{x+1,y,z} + p_{x-1,y,z} - 2p_{x,y,z}}{(\triangle x)^2} + \\
&\quad \frac{p_{x,y+1,z} + p_{x,y-1,z} - 2p_{x,y,z}}{(\triangle x)^2} + \\
&\quad \frac{p_{x,y,z+1} + p_{x,y,z-1} - 2p_{x,y,z}}{(\triangle x)^2} \\
&= \frac{p_{x+1,y,z} + p_{x-1,y,z} + p_{x,y+1,z} + p_{x,y-1,z} + p_{x,y,z+1} + p_{x,y,z-1} - 6p_{x,y,z}}{(\triangle x)^2}
\end{aligned}
\tag{3.1}
$$

where $\triangle x$ is the edge length of the cubic cell.

For the velocity field $\mathbf{u}$, a slightly more sophisticated method known as the **MAC** (Marker and Cell) grid is used. Instead of storing the value of $\mathbf{u} = (\mathbf{u}_x, \mathbf{u}_y, \mathbf{u}_z)$ sampled at the cell center, an MAC grid stores different components of $\mathbf{u}$ sampled at different locations. Specifically, the grid cell at position (x, y, z) stores the value of $\mathbf{u}_x$ sampled at the center of its left face, the value of $\mathbf{u}_y$ sampled at its lower face, and the value of $\mathbf{u}_z$ sampled at its back face, as illustrated in this figure:

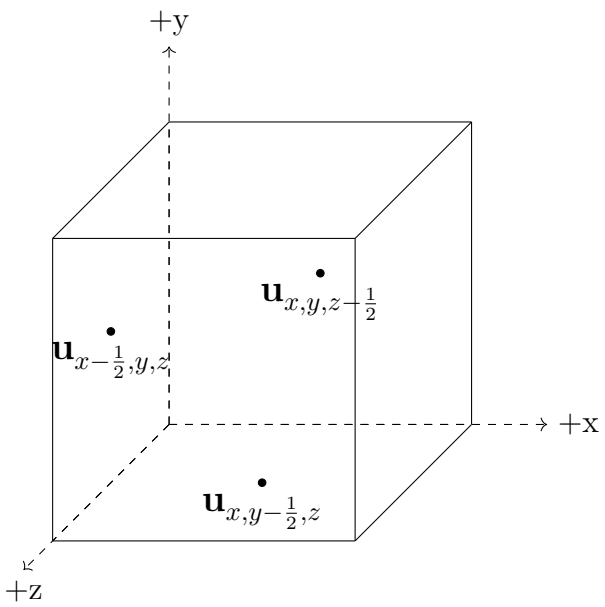

Figure 3.1: a 3D MAC grid cell and the velocity data it stores

The quantities $\mathbf{u}_{x,y,z-\frac{1}{2}}$, $\mathbf{u}_{x,y-\frac{1}{2},z}$, $\mathbf{u}_{x-\frac{1}{2},y,z}$ are all scalars, representing the velocity pointing at the x, y, and z direction, respectively. Furthermore, notice that the values of $\mathbf{u}_{x+\frac{1}{2},y,z}$, $\mathbf{u}_{x,y+\frac{1}{2},z}$, and $\mathbf{u}_{x,y,z+\frac{1}{2}}$, which are respectively sampled at the centers of

the right, upper, and front faces, will also be available. This is because $\mathbf{u}_{x+\frac{1}{2},y,z} = \mathbf{u}_{x+1-\frac{1}{2},y,z}$, that is, the value of $\mathbf{u}_x$ sampled at the right face of the cell is exactly the value of $\mathbf{u}_x$ sampled at the left face of the neighboring cell on the right. The same can be applied for the upper and front faces. As a result, there are 6 velocity values associated with each grid cell:

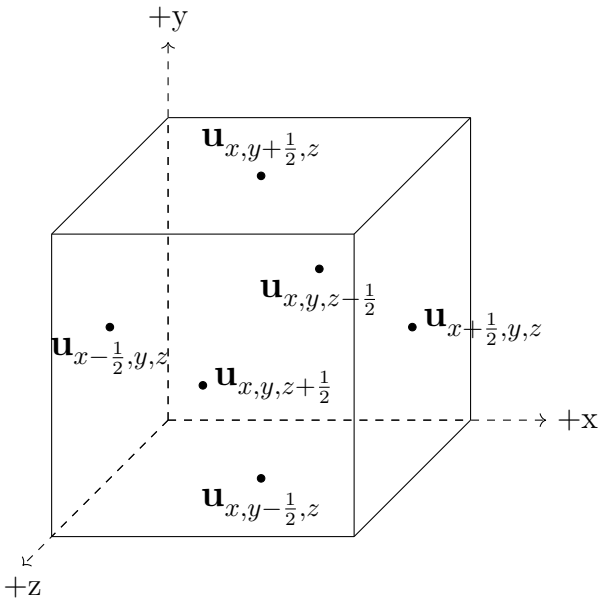

Using these quantities, an approximation of the divergence of the velocity, $\nabla \cdot \mathbf{u}$, sampled at cell centers, can be easily computed:

$$\begin{aligned}
\nabla \cdot \mathbf{u} &= \frac{\partial \mathbf{u}_x}{\partial x} + \frac{\partial \mathbf{u}_y}{\partial y} + \frac{\partial \mathbf{u}_z}{\partial z} \\
&\approx \frac{\triangle \mathbf{u}_x}{\triangle x} + \frac{\triangle \mathbf{u}_y}{\triangle y} + \frac{\triangle \mathbf{u}_z}{\triangle z} \\
&= \frac{\mathbf{u}_{x+\frac{1}{2},y,z} - \mathbf{u}_{x-\frac{1}{2},y,z}}{\triangle x} + \frac{\mathbf{u}_{x,y+\frac{1}{2},z} - \mathbf{u}_{x,y-\frac{1}{2},z}}{\triangle x} + \frac{\mathbf{u}_{x,y,z+\frac{1}{2}} - \mathbf{u}_{x,y,z-\frac{1}{2}}}{\triangle x}
\end{aligned} \tag{3.2}$$

During the incompressibility step of the simulation, the velocity field will be updated according to the gradient of the pressure field. Thus, it is also important to compute the approximation of ∇p at the velocity field sample points, i.e., the centres of faces of the cells. This is made easy by the fact that the pressure field is sampled at the cells' centres:

$$(\nabla p)_{x-\frac{1}{2},y,z} = \frac{p_{x,y,z} - p_{x-1,y,z}}{\triangle x} \tag{3.3}$$

The numerical approximations to $\nabla \cdot \nabla p$, $\nabla \cdot \mathbf{u}$, and ∇p will all be used during the incompressibility step, as will be explained in section 3.5.

3.3 Advection

As previously explained, the first step in each time step of the simulation is to solve the advection equation $\frac{D\mathbf{u}}{Dt} = 0$. Intuitively, this equation demands that the velocity of each infinitesimal particle in the fluid remains unchanged (but the velocity field itself will change because the positions of the particles will change).

A once widely used advection algorithm is called **PIC** (Particle in Cell), which is closely based on the intuition behind the material derivative. Instead of infinitely many infinitely small particles, the fluid is approximately represented using a finite but large cloud of particles, each storing its own velocity. Using the velocity field $\mathbf{u}_{[n]}$ in nth time step, the PIC advection at the $n+1$ th time step works in these following steps:

1. For each particle p with position $\mathbf{x}_p$, sample and interpolate the MAC grid to obtain the value of $\mathbf{u}_{[n]}$ at $\mathbf{x}_p$. Assign this as the particle's velocity, $\mathbf{u}_p$.

2. Move the particle in the velocity field $\mathbf{u}_{[n]}$. This can be as simple as computing $\mathbf{x}_p^{new} = \mathbf{x}_p + \triangle t \mathbf{u}_{[n]}(\mathbf{x}_p)$. For higher accuracy, this project performs this using a 3rd-order Runge-Kutta integration:

$$\begin{aligned}
\mathbf{u}_{temp1} &= \mathbf{u}_{[n]}(\mathbf{x}_p) \\
\mathbf{u}_{temp2} &= \mathbf{u}_{[n]}(\mathbf{x}_p + \frac{1}{2}\triangle t \mathbf{u}_{temp1}) \\
\mathbf{u}_{temp3} &= \mathbf{u}_{[n]}(\mathbf{x}_p + \frac{3}{4}\triangle t \mathbf{u}_{temp2}) \\
\mathbf{x}_p^{new} &= \mathbf{x}_p + \triangle t(\frac{2}{9}\mathbf{u}_{temp1} + \frac{3}{9}\mathbf{u}_{temp2} + \frac{4}{9}\mathbf{u}_{temp3})
\end{aligned}$$

   For particles near the fluid boundaries, some of the $\mathbf{u}_{temp}$ values might be sampled outside the fluid region, which is slightly problematic because the velocity isn't defined outside the fluids. This is fixed by a simple *extrapolation* step, which extends the velocity to a few grid cells outside its original region.

3. For each MAC grid cell, and for each of its 3 sample points where a component of $\mathbf{u}$ is stored, find all particles within a certain small radius (usually $\triangle x$), and interpolate their value of $\mathbf{u}_p$. Save these values as a temporary velocity field, $\mathbf{u}_{[n+1]}^{advected}$.

In short, the PIC algorithm first transfers the velocity field from the MAC grid to the particles, then moves the particles, and finally transfers the velocity from the particles back to the MAC grid.

The PIC algorithm is largely superseded by another algorithm known as **FLIP** (Fluid Implicit Particle), which is implemented in this project. FLIP is very similar to PIC, with only a slightly different 1st step:

1′. For each particle p with position $\mathbf{x}_p$, sample and interpolate the MAC grid to obtain the value of $\mathbf{u}_{[n]} - \mathbf{u}_{[n-1]}$ at $\mathbf{x}_p$. Add this to the particle's velocity, $\mathbf{u}_p$.

That is, instead of interpolating the value of $\mathbf{u}$ on to the particles, FLIP interpolates the change of $\mathbf{u}$ in the last time step, and adds that to the particles' velocities. Zhu and Bridson[20] showed that this method reduces the undesirable effect called *numerical dissipation*, where visually interesting details in the fluid are smoothed away due to excessive interpolation.

3.4 External Forces

After obtaining the temporary velocity field $\mathbf{u}_{[n+1]}^{advected}$, the next step is to apply external forces. Two types of external forces will be considered: the forces arising from an external force field such as gravity, and the forces exerted by a solid boundary.

Let $\mathbf{g}$ denote the acceleration caused by the external force field, (for gravity, $\mathbf{g} \approx [0, -0.98, 0]^T$), applying the forces is then achieved by adding $\triangle t\mathbf{g}$. In a MAC grid, this is done by updating the components of $\mathbf{u}$ sampled at different faces using the different components of $\triangle t\mathbf{g}$.

To apply the solid boundary condition $\mathbf{u} \cdot \mathbf{n} = 0$, as mentioned in section 2.4, components of $\mathbf{u}$ sampled at faces that represent solid-fluid boundaries need to be set to 0. For example, if the solid region is considered to be exactly the region of space outside the MAC grid, then the leftmost faces of the leftmost cells (and rightmost faces of rightmost cells...etc.) will be considered as a solid-fluid boundary. For all such boundary faces, the velocity component there will be set to 0.

Starting from an incompressible velocity field $\mathbf{u}_{[n]}$, performing advection to obtain $\mathbf{u}_{[n+1]}^{advected}$, and then applying external forces, the resulting velocity will likely not be incompressible anymore. Let this field be called $\mathbf{u}_{[n+1]}^{compressible}$, and the next step will be to apply pressure within the fluid, so that the incompressibility is restored.

3.5 Enforcing Incompressibility

To enforce the incompressibility condition $\nabla \cdot \mathbf{u}_{[n+1]} = 0$, the algorithm needs to find a pressure field p such that,

$$\nabla \cdot \mathbf{u}_{[n+1]} = \nabla \cdot (\mathbf{u}_{[n+1]}^{compressible} - \triangle t \frac{\nabla p}{\rho}) = 0$$

Rearranging the equation on the right gives

$$-\frac{\triangle t}{\rho} \nabla \cdot \nabla p = -\nabla \cdot \mathbf{u}_{[n+1]}^{compressible} \tag{3.4}$$

Using the discretization formulas 3.1 and 3.2, the discrete version of this equation can be written:

$$\begin{aligned} &\frac{\triangle t}{\rho \triangle x}(6p_{x,y,z} - p_{x+1,y,z} - p_{x-1,y,z} - p_{x,y+1,z} - p_{x,y-1,z} - p_{x,y,z+1} - p_{x,y,z-1}) \\ &\quad = -(\mathbf{u}_{x+\frac{1}{2},y,z} - \mathbf{u}_{x-\frac{1}{2},y,z} + \mathbf{u}_{x,y+\frac{1}{2},z} - \mathbf{u}_{x,y-\frac{1}{2},z} + \mathbf{u}_{x,y,z+\frac{1}{2}} - \mathbf{u}_{x,y,z-\frac{1}{2}}) \end{aligned} \tag{3.5}$$

One such equation exists for every cell that contains fluid (i.e contains FLIP particles), and together, they form a system of linear equations, called the *Poisson pressure equation*. The unknowns, $p_{i,j,k}$, correspond to the pressure at the centers of cells.

Since each equation involves not only the pressure of the fluid cell itself, but also the pressure of its 6 adjacent cells, extra care needs to be taken for cells that are at the boundaries of the fluid. Specifically, if a variable $p_{i,j,k}$ in the equations corresponds to the pressure within an air cell, it should automatically be assigned 0, which satisfies the free-surface boundary conditions. If the variable $p_{i,j,k}$ corresponds to the pressure within solid, then it suffices to replace it with the pressure of the fluid cell next to the boundary, because the velocities at solid-fluid boundaries were already fixed in the external forces step.

With the boundary conditions satisfied, the equation becomes a system of N linear equations with N variables, where N is the total amount of fluid cells. Solving this system hence results in a discrete representation of the pressure field p that satisfies

$$\nabla \cdot (\mathbf{u}_{[n+1]}^{compressible} - \triangle t \frac{\nabla p}{\rho}) = 0$$

Then, to retrieve the incompressible velocity field, it only remains to compute

$$\mathbf{u}_{[n+1]} = \mathbf{u}_{[n+1]}^{compressible} - \triangle t \frac{\nabla p}{\rho}$$

using discretization formula 3.2. This completes the simulation of one time step.

To summarize, using a grid and FLIP advection, the simulation of each time step follows the following procedure:

Algorithm 1: Single phase fluid FLIP simulation step

```
// At time step [n+1]
```
foreach *particle* p **do**
  $\mathbf{u}_p := \mathbf{u}_p + \mathbf{u}_{[n]}(\mathbf{x}_p) - \mathbf{u}_{[n-1]}(\mathbf{x}_p)$;
  Move p inside the velocity field using Runge-Kutta;
end
foreach *grid cell at location* (x, y, z) **do**
  Find all particles within a radius of $\triangle x$;
  Compute $\mathbf{u}_{[n+1]}^{advected}$, as an interpolation of the $\mathbf{u}_p$ of nearby particles;
end
Apply external forces, $\mathbf{u}_{[n+1]}^{compressible} = FixSolidBoundary(\mathbf{u}_{[n+1]}^{advected} + \triangle t\mathbf{g})$;
Solve the Poisson pressure equation to obtain pressure p;
Compute $\mathbf{u}_{[n+1]} = \mathbf{u}_{[n+1]}^{compressible} - \triangle t\frac{\nabla p}{\rho}$

3.6 Multiphase Fluid Simulation

While algorithm 1 is only for single-phase fluid simulation, it is possible to extend it to support multiple fluid phases. As explained in section 2.5, the changes in the concentration α^i of a fluid phase i are governed by the Advection-Diffusion equation:

$$\frac{D\alpha^i}{Dt} = C\nabla \cdot \nabla\alpha^i$$

To incorporate this equation into the simulation algorithm, the first step is again to apply splitting. The equation is split into two parts:

$$\frac{D\alpha^i}{Dt} = 0$$
$$\frac{\partial\alpha^i}{\partial t} = C\nabla \cdot \nabla\alpha^i$$

Just like the Euler momentum equation, this first equation that splitting produces is an advection equation. Thus, the same FLIP advection that was applied for the velocity field can be used to advect the concentration quantities: first transfer the quantities from the grid to the particles by interpolating and adding $\alpha_{[n]}^i - \alpha_{[n-1]}^i$, then move the particles in the velocity field, then transfer the α^i back to the grid.

The second equation is the "diffusion" part of the advection-diffusion equation, and is sometimes referred as the diffusion equation by itself. It was shown that

using forward Euler scheme for this equation is unstable for large time steps[7], so a discretized implicit equation is used:

$$\begin{aligned} -\lambda\alpha^i_{[n+1]\ x-1,y,z} - \lambda\alpha^i_{[n+1]\ x+1,y,z} \\ -\lambda\alpha^i_{[n+1]\ x,y-1,z} - \lambda\alpha^i_{[n+1]\ x,y+1,z} \\ -\lambda\alpha^i_{[n+1]\ x,y,z-1} - \lambda\alpha^i_{[n+1]\ x,y,z+1} \\ +(1+6\lambda)\alpha^i_{[n+1]x,y,z} \end{aligned} \quad = \quad \alpha^{i,advected}_{[n]x,y,z} \tag{3.6}$$

where $\lambda = \dfrac{C\triangle t}{(\triangle x)^2}$. With the value of α^i_{n+1} at each fluid cell as unknown, this is again a linear equation. Solving this equation produces the new concentration field, $\alpha^i_{[n+1]}$.

Furthermore, with multiphase support, the incompressibility step in the original FLIP requires a small modification. Since different fluid phases are allowed to have different densities, the value ρ in the pressure Poisson equation 3.4 is no longer a constant, but a scalar field that varies. This requires ρ to also be stored in a grid, and for each sample location $\mathbf{x}$, it is calculated by

$$\rho(\mathbf{x}) = \sum_i \rho^i \alpha^i(\mathbf{x})$$

where ρ^i is the constant density of the ith fluid phase.

Incorporating the FLIP concentration advection and the diffusion equation into the algorithm 1, a new algorithm is created, which supports multiphase fluid simulation:

Algorithm 2: Multiphase phase fluid FLIP simulation step

```
// At time step [n+1]
```
foreach *particle p* **do**
  $\mathbf{u}_p := \mathbf{u}_p + \mathbf{u}_{[n]}(\mathbf{x}_p) - \mathbf{u}_{[n-1]}(\mathbf{x}_p)$;
  $\boldsymbol{\alpha}_p := \boldsymbol{\alpha}_p + \boldsymbol{\alpha}_{[n]}(\mathbf{x}_p) - \boldsymbol{\alpha}_{[n-1]}(\mathbf{x}_p)$;
  Move p inside the velocity field using Runge-Kutta;
end
foreach *grid cell at location* (x, y, z) **do**
  Find all particles within a radius of $\triangle x$;
  Compute $\mathbf{u}^{advected}_{[n+1]}$, as an interpolation of the $\mathbf{u}_p$ of nearby particles;
  Compute $\boldsymbol{\alpha}^{advected}_{[n+1]}$, as an interpolation of the $\boldsymbol{\alpha}_p$ of nearby particles;
end
Apply external forces, $\mathbf{u}^{compressible}_{[n+1]} = FixSolidBoundary(\mathbf{u}^{advected}_{[n+1]} + \triangle t\mathbf{g})$;
Solve the Poisson pressure equation to obtain pressure p;
Compute $\mathbf{u}_{[n+1]} = \mathbf{u}^{compressible}_{[n+1]} - \triangle t\dfrac{\nabla p}{\rho}$;
Solve the diffusion equation to obtain $\boldsymbol{\alpha}_{n+1}$.

4 Implementing FLIP

In order to achieve real-time simulation, algorithm 2 needs to be executed at maximum performance. This project approaches this by exploiting the parallel computing power of modern GPUs. This chapter begins by giving a short introduction to GPU computing, and then explains the parallel version of algorithm 2 designed and implemented in this project. Some special GPU memory access optimizations in the implementation, which considerably boosted the efficiency of the simulation, are also discussed.

4.1 The CUDA Programming Model

Originally built for graphics applications, GPUs are designed to handle a massive amount of geometries and pixels in parallel, because in graphics applications the computations for different geometries and pixels are largely independent. The ability to do massively parallel computation motivated GPGPU (General-Purpose GPU) programming models to arise, which became significantly useful for scientific computing purposes. The software in this project is written using the CUDA programming model, developed by the NVIDIA Corporation.

CUDA employs the execution model known as SIMT (Single Instruction Multiple Threads). In this model, a large amount of GPU threads can be spawned simultaneously, each running the same sequence of code on different sets of data. GPU threads in CUDA are organized in groups of 32, known as *warps*, and the instructions running on threads of the same warp must be synchronized. However, different warps do not need to remain in sync. When the threads within a warp access the memory, the entire warp can be paused and swapped out, so that a different warp can start executing before the memory access finishes. Using this mechanism, the GPU hides memory access latencies by allowing very fast context switching. As a result, each physical core in the GPU (known as a CUDA core) can simultaneously handle multiple logical threads.

As an example, the GPU used for development of this project is an NVIDIA GTX1060 Mobile, which contains 10 *Streaming Multiprocessors*, each of which consists of 128 CUDA cores. Each streaming multiprocessors can have up to 2048 resident threads, giving a total of 20480 threads that can be simultaneously handled. Even though each GPU thread is not as fast as a CPU thread, the aggregated performance of the CUDA cores can still be many times faster than the CPU.

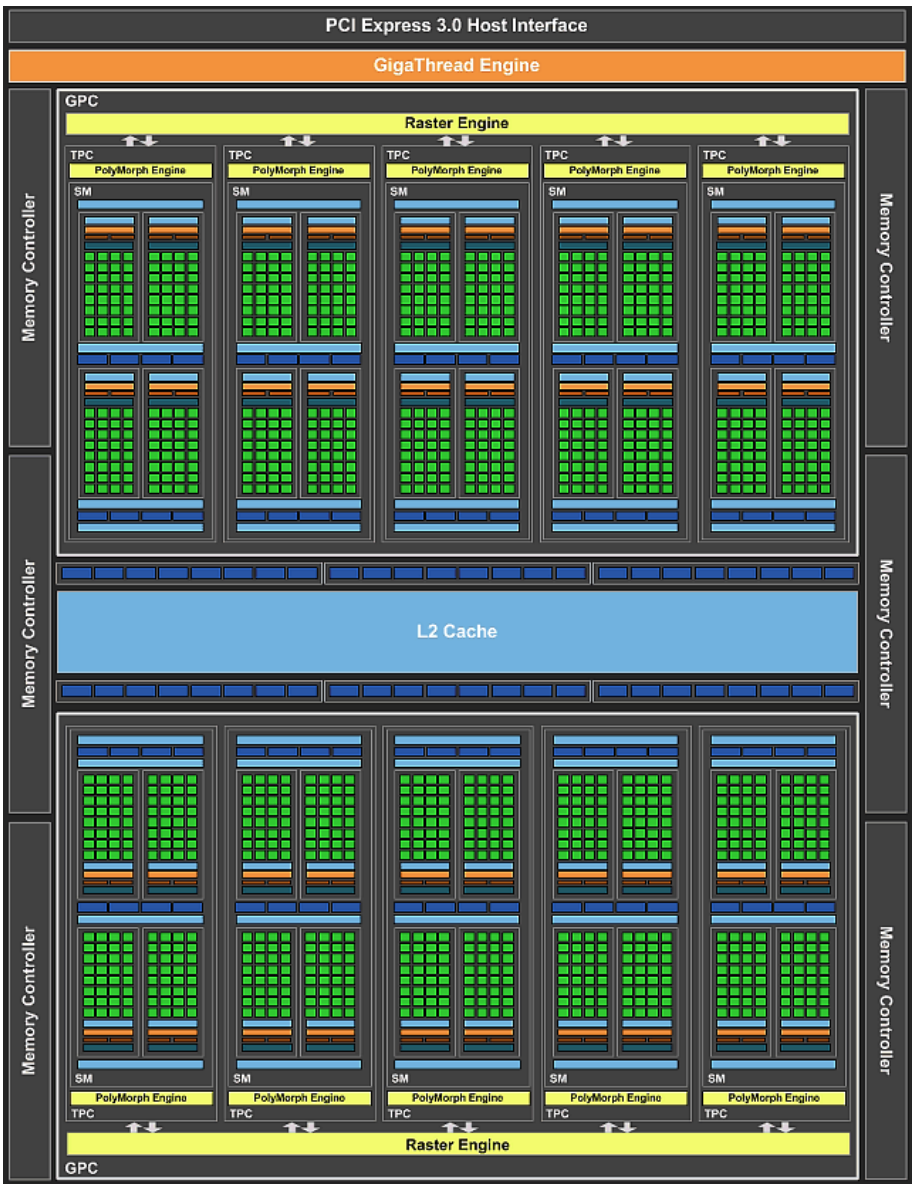

Figure 4.1: Architecture of a GTX 1060 (GP106), showing its 10 streaming multiprocessors, each containing 128 CUDA cores. Image courtesy to NVIDIA Corporation.

4.2 Parallelization

The pseudocode representation of algorithm 2 takes a sequential form, so in order to create an efficient CUDA implementation, the challenge remains to parallelize the algorithm.

For certain parts of the algorithm, parallelization is straightforward. Examples include lines 2-4 and lines 8-9 within the pseudocode. These are all operations performed within a loop body, with the convenient property that, in different loop iterations, the data being operated on are completely different, and do not depend on previous iterations. This means it is safe to use parallel threads instead of actual loops to perform these operations. Similarly, the velocity field updates in line 11 and 13 are also easy to parallelize, with each thread operating on one grid cell of the discretized velocity field.

The rest of the algorithm, lines 7, 12, and 14, requires much more attention. Line 7 performs a task called *spatial indexing*: associating each grid cell with all the particles that are within radius $\triangle x$ at each time step. A naive implementation would require a linear search on all particles, and this has to be performed for all grid cells, which is intolerable because the simulation could involve up to around 1,000,000 particles and 100,000 grid cells. In lines 12 and 14, a linear equation needs to be solved, where there is an unknown for each fluid cell. As a result, the total amount of unknowns is in the order of 100,000. A naive linear solver would have an $O(N^3)$ complexity, which is also too costly. Each of these operations, indexing 1,000,000 million particles and solving linear equations with 100,000 unknowns, needs to be performed at least around 20 times per second, if the simulation is to be performed in real time. This section will focus on how this is made possible in this project.

4.2.1 Spatial Indexing

With $\triangle x$ being the edge length of each cubic grid cell, finding all particles within a radius $\triangle x$ of each cell can be reduced to finding the particles that are *inside* each cell. Then, for a certain cell, it suffices to check all the 27 cells in the neighbourhood, because all particles within a radius $\triangle x$ must be contained inside these 27 cells.

To create an index from each cell to the particles inside the cell, this project uses the parallel algorithm proposed by Green[5]. The algorithm proceeds in the following steps:

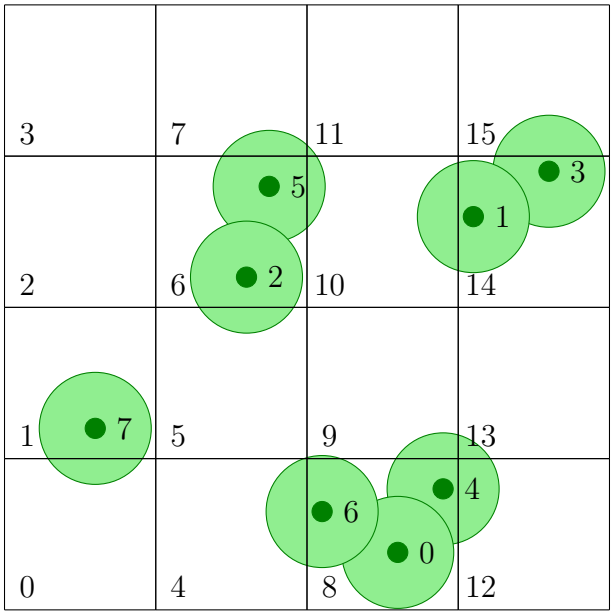

(a) The indices and positions of the particles in the grid before spatial indexing.

particle	hash
0	8
1	14
2	6
3	14
4	8
5	6
6	8
7	1

(b) The array of hashes of particles, computed in step 2.

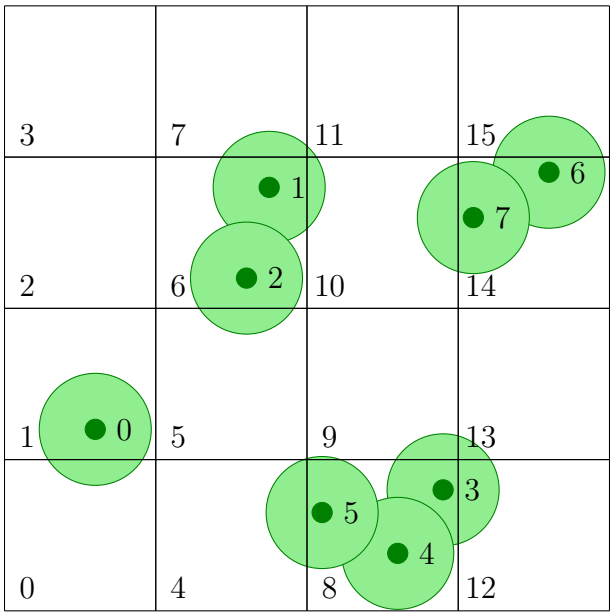

(c) The indices and positions of the particles, after they are sorted according to their hashes, in step 3.

cell	*cellStart*	*cellEnd*
0		
1	0	0
2		
3		
4		
5		
6	1	2
7		
8	3	5
9		
10		
11		
12		
13		
14	6	7
15		

(d) The final result of spatial indexing, represented as the *cellStart* and *cellEnd* array.

Figure 4.2: Example of spatial indexing in 2D

1. Decide on a hash function for 3D grid coordinates. For example, in an $N*N*N$ grid, the hash of the coordinate (x, y, z) can be xN^2+yN+z, which fully avoids hash collision.

2. Create an array of hashes for particles. For each particle, use its physical position to compute the cell that it is in, and compute the hash of that cell as the hash of the particle. Store the hashes of all particles in this array. Since this step is independent for each particle, it can be efficiently parallelized.

3. Sort this array of particle hashes, and sort the array of particles into the same order.

4. Create two arrays *cellStart* and *cellEnd*, which denote, for each cell, the first and the last particle inside the cell. To compute elements of these arrays, for the ith particle, use the hash array to check if the $i-1$th particle is in the same cell, if not, the *cellStart* of this cell should be i. Similarly, if the $i+1$th particle is not in the same cell, the *cellEnd* of this cell should be i. This can also be done for all particles in parallel.

A 2D example of this procedure is illustrated in figure 4.2.

Having created the *cellStart* and *cellEnd* arrays, the particles in the cth cell can now be found as precisely the ones with index $\geq cellStart[c]$ and $\leq cellEnd[c]$. Thus, this allows instant access to neighbor particles, given spatial coordinates.

With all other steps being completely parallelizable, the only complicated step is sorting the array of particle hashes. The implementation of this project uses the thoroughly optimized sorting library provided with the CUDA API. The resulting cost of the spatial indexing is almost negligible compared to other tasks, such as solving systems of linear equations.

4.2.2 Jacobi Linear Solver

The two linear systems to be solved in each simulation step, the Poisson pressure equation and the diffusion equation, both have the special property of being *symmetric positive-definite*. Many advanced approaches have been proposed on how to solve these types of matrices, such as ICPCG [3] and *Geometric Multigrid*[4]. This project chooses to implement a simpler algorithm, called the Jacobi solver. Though not as fast as the most advanced methods, its efficiency and accuracy are found to be sufficient for the real-time simulations in this project.

In the Jacobi Solver, given a system of linear equations written in matrix form:

$$A\mathbf{x} = \mathbf{b}$$

the matrix A is decomposed into $D + C$, where D is a diagonal matrix, and C has only 0s on the diagonal:

$$(D + C)\mathbf{x} = \mathbf{b}$$

The system is then rewritten as

$$D\mathbf{x} = \mathbf{b} - C\mathbf{x}$$

Thus,

$$\mathbf{x} = D^{-1}(\mathbf{b} - C\mathbf{x})$$

which motives an iterative scheme: begin with an initial guess $\mathbf{x}_0$, and then iteratively compute

$$\mathbf{x}_{i+1} = D^{-1}(\mathbf{b} - C\mathbf{x}_i) \tag{4.1}$$

For a certain amount of iterations. The computations of this formula for different unknowns (different components of $\mathbf{x}_{i+1}$) are completely independent. Therefore, by designating a CUDA thread for each unknown (and thus, for each cell), the Jacobi iteration step is completely parallelized.

Additionally, by observing the pressure equation 3.5 and the diffusion equation 3.6, a further simplification can be made, because the matrix C corresponding to these equations has some convenient properties. For the unknown x corresponding to each cell, the row of C corresponding to that cell only has non-zero entries for immediately adjacent cells. Consequently, for each cell, the computation of formula 4.1 only requires sampling the x at adjacent cells. This leads to a highly parallel implementation of the Jacobi iteration:

Algorithm 3: Parallel Jacobi Iteration

foreach *grid cell* ***in parallel*** **do**
- Let the coordinate of the cell be (i, j, k);
- Retrieve the scalars $D_{(i,j,k)}$ and $b_{(i,j,k)}$;
- $neighborValues := 0$;
- Sample the left cell: $neighborValues \mathrel{+}= C_{(i-1,j,k)}\ x_{(i-1,j,k)}$;
- Sample the right cell: $neighborValues \mathrel{+}= C_{(i+1,j,k)}\ x_{(i+1,j,k)}$;
- Sample the lower cell: $neighborValues \mathrel{+}= C_{(i,j-1,k)}\ x_{(i,j-1,k)}$;
- Sample the upper cell: $neighborValues \mathrel{+}= C_{(i,j+1,k)}\ x_{(i,j+1,k)}$;
- Sample the back cell: $neighborValues \mathrel{+}= C_{(i,j,k-1)}\ x_{(i,j,k-1)}$;
- Sample the front cell: $neighborValues \mathrel{+}= C_{(i,j,k+1)}\ x_{(i,j,k+1)}$;
- Update $x_{(i,j,k)} := (b_{(i,j,k)} - neighborValues)/D_{(i,j,k)}$

end

Using the parallel spatial indexing algorithm and the Jacobi linear solver, the updated FLIP algorithm is now described as:

Algorithm 4: Parallel multiphase phase fluid FLIP simulation step

```
   // At time step [n+1]
 1 foreach particle p in parallel do
 2 |   u_p := u_p + u_[n](x_p) − u_[n−1](x_p) ;
 3 |   α_p := α_p + α_[n](x_p) − α_[n−1](x_p) ;
 4 |   Move p inside the velocity field using Runge-Kutta;
 5 end
 6 Perform spatial indexing;
 7 foreach grid cell at location (x, y, z) in parallel do
 8 |   Compute u^advected_[n+1], as an interpolation of the u_p of nearby particles;
 9 |   Compute α^advected_[n+1], as an interpolation of the α_p of nearby particles;
10 end
11 foreach grid cell at location (x, y, z) in parallel do
12 |   Apply external forces at the cell:
   |     u^compressible_[n+1] = FixSolidBoundary(u^advected_[n+1] + △t g);
13 end
14 Using Jacobi, solve the Poisson pressure equation to obtain pressure p;
15 foreach grid cell at location (x, y, z) in parallel do
16 |   Compute the new velocity field at the cell: u_[n+1] = u^compressible_[n+1] − △t ∇p/ρ;
17 end
18 Using Jacobi, solve the diffusion equation to obtain α_[n+1].
```

This parallel formulation of the multiphase FLIP algorithm is now ready to be implemented in CUDA.

4.3 Optimizing Grid Access

While writing the CUDA code for algorithm 4, many optimizations are still possible. This section describes one of the most effective optimizations that was made in this project, which is to use a special type of GPU memory, called the *texture* memory, for storing the discrete grids.

The key observation behind this optimization is that, algorithm 4 very often performs the operation of accessing the values stored in multiple adjacent grid cells. This happens during advection, in lines 2-4, where the velocity field $\mathbf{u}$ and concentration field $\boldsymbol{\alpha}$ is sampled at the locations of particles, and thus an interpolation of all nearby MAC sample points is required. This also occurs at lines 14 and 18, inside the Jacobi

solver. As presented in algorithm 3, in each Jacobi iteration, the thread for each cell samples the values of its 6 adjacent cells. The advection and Jacobi solver are in fact the most costly steps in the simulation, which hints that if it is possible to speed up the access of multiple adjacent grid cells, the performance of the entire algorithm could be noticeably improved.

This memory access pattern as described exhibits *spatial locality*. However, this is not in the sense of the normal 1D address space locality often discussed in the context of CPU programming, but rather a locality in the 3D space. Fortunately, this specific pattern is in fact quite common in traditional computer graphics applications, where operations such as image filtering are constantly performed. GPUs are thus equipped with a special type of memory, called the *texture* memory, which accelerates these operations. A texture memory maps the 3D grid onto a type of *space-filling curve*, where adjacent points in the 3D space often correspond to adjacent points on the curve. A 2D example of such a curve is:

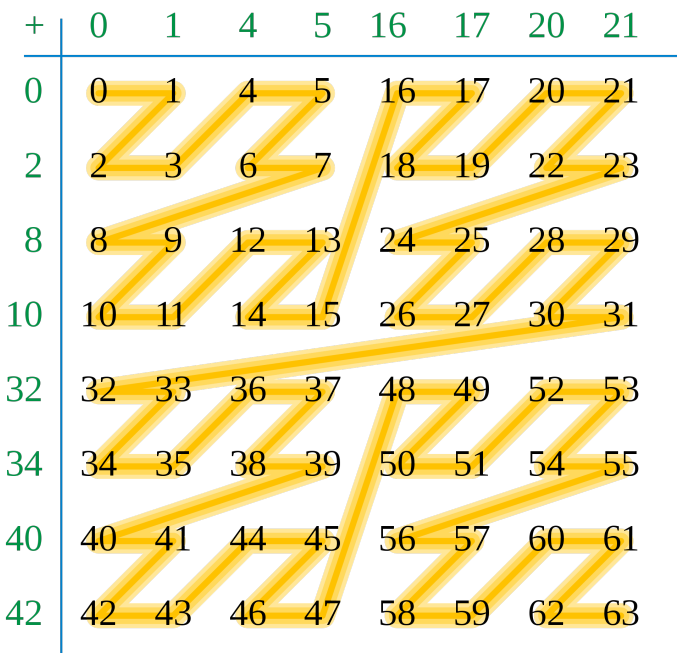

Figure 4.3: A Z-order curve. Image courtesy to Wikipedia

Using a space-filling curve, the texture memory converts the desired 2D/3D spatial locality into 1D locality, which allows the memory access to be more cache-friendly.

5 Rendering

In computer graphics applications, the ultimate goal for fluid simulation is usually so that the fluid can be rendered and displayed to the human user. Thus, in addition to the FLIP simulation, this project also implements a rendering procedure, so that the simulation and rendering and be conducted together in real time. This chapter introduces the key rendering facilities that are implemented and the algorithms used.

5.1 The OpenGL Drawing Pipeline

This project uses the OpenGL API for rendering. OpenGL is a widely used standard to program the GPU for graphics purposes, and just like any other graphics API (e.g. Direct3D, Vulkan), the only types of geometric primitives that can be drawn are points, lines, and triangles. For this reason, in order to render complex 3D objects, a mesh of triangles is often used to represent the surface of the object. In OpenGL's pipeline, these triangles undergo 4 main stages of computation on the GPU:

1. *The Vertex Shader*

   The vertex shader is a piece of GPU program (usually written in GLSL), and it is executed for each vertex of every triangle to be rendered. Usually, the vertex shader computes essential geometric information (e.g. normal vector, position on screen) of the vertices, which are passed on to the next stage.

2. *Rasterization*

   During rasterization, a piece of GPU hardware uses the screen positions of vertices to determine, for each triangle, which pixels are within the triangle. Each pixel of each triangle is then passed on to the next stage for colouring.

3. *The Pixel Shader*

   Also referred to as the *fragment shader*, the pixel shader is also a piece of GPU program. The pixel shader culminates the job of the entire graphics pipeline: it computes the colour of each pixel to be displayed.

4. *Compositing*

   In 3D scenes, objects might hide behind each other, and some pixels might be covered by multiple objects at different depths. The compositor's job is to determine which shading of the pixel should be used, and in some cases (e.g. when rendering translucent objects), how the differently shaded colours should be mixed together to give the final output. This process is essential to the multiphase fluid rendering algorithm invented in this project, to be described in subsection 5.3.2.

The full OpenGL pipeline includes a few extra stages, such as the geometry shader and the tesselation shader. However, these are optional stages and are not used in this project.

5.2 Surface Reconstruction

To render liquids, the first step is to represent the surface of the liquid as a mesh of triangles, which can then be fed into the GPU rendering pipeline. Since this triangle mesh is not maintained by the simulation algorithms, it needs to be generated in each frame. This project implements an algorithm that uses the cloud of FLIP particles, which occupy the entire fluid region, to generate these triangles.

In the paper where they also described FLIP[20], Zhu and Bridson utilized a concept called *Signed Distance Field* to perform surface reconstruction. The signed distance field $\phi : \mathbb{R}^3 \to \mathbb{R}$ is a scalar field, with the property that, given a 3D cartesian coordinate $\mathbf{x}$:

- $\phi(\mathbf{x}) = 0$ if $\mathbf{x}$ is on the boundary of the fluid region.
- $\phi(\mathbf{x}) = d$ if $\mathbf{x}$ is outside the fluid region, and the shortest distance between $\mathbf{x}$ and any point on the surface is d.
- $\phi(\mathbf{x}) = -d$ if $\mathbf{x}$ is inside the fluid region, and the shortest distance between $\mathbf{x}$ and any point on the surface is d.

Thus, the magnitude of $\phi(\mathbf{x})$ indicates the distance between $\mathbf{x}$ and the surface, and the sign of $\phi(\mathbf{x})$ indicates whether $\mathbf{x}$ is in the inside or outside. The fluid surface is then precisely the set of points where ϕ evaluates to 0. In literature, this is often called the *zero-isocontour* or *zero-isosurface*.

Zhu and Bridson's method[20] begins by considering the special case where there is only a single particle in the fluid. Assume the particle is centered at $\mathbf{x}_0$ and has radius r_0, the signed distanced field of this spherical fluid region must then be:

$$\phi(\mathbf{x}) = ||\mathbf{x} - \mathbf{x}_0|| - r_0$$

This is then generalized to N particles, where $\mathbf{x}_0$ is replaced by a weighted average of the center positions of nearby particles:

$$\begin{aligned} \phi(\mathbf{x}) &= ||\mathbf{x} - \overline{\mathbf{x}}|| - r \\ \overline{\mathbf{x}} &= \frac{\sum_{i=1}^{N} W(\mathbf{x} - \mathbf{x}_i, h)\mathbf{x}_i}{\sum_{i=1}^{N} W(\mathbf{x} - \mathbf{x}_i, h)} \end{aligned} \tag{5.1}$$

where it is assumed that all particles have the same radius r. The W is a bell-shaped kernel function, which weights the contribution of all particles within a radius of h. Particles beyond this distance are given a weight of 0. This project chooses h to be $2\triangle x$, and uses the W proposed by Zhu and Bridson:

$$W(\mathbf{r}, h) = max(0, (1 - \frac{||\mathbf{r}||^2}{h^2})^3)$$

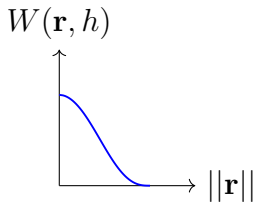

Using formula 5.1, a discretized signed distance field can be computed and stored on a 3D grid. Notice that since the computation of $\overline{\mathbf{x}}$ sums over neighbor particles, the spatial indexing technique described in section 4.2.1 will again be needed when implementing the formula. The discrete grid of ϕ values is often called a *level set*[3].

Having computed the discrete signed distance field ϕ, it remains to extract its zero-isosurface as a triangle mesh. This is done using a famous algorithm called *Marching Cubes*, invented by Wyvill[18] and Lorensen[9]. The algorithm considers each cubic grid cell in the level set grid, and puts a triangle vertex at each edge of the cube if one end of the edge is outside the fluid($\phi > 0$) and the other end is inside the fluid ($\phi \leq 0$). Since each cube has 8 vertices, and each vertex can be either inside or outside the fluid, there're a total of $2^8 = 256$ different cases for each cube. A selection of them is shown in the following figure:

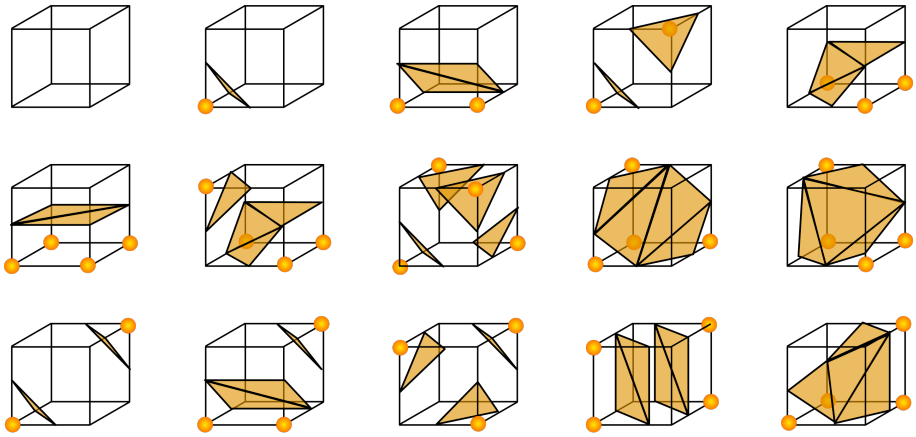

Figure 5.1: 15 of the 256 cases for each cube. The coloured vertices are the ones inside the fluid. The orange triangles are the results generated for each cube. Image courtesy of the Wikipedia page on Marching Cubes.

The triangles generated for all the cells connect together into a watertight mesh, which can be fed into the OpenGL pipeline for rendering. This project implements the Marching Cubes algorithm by using a precomputed lookup table, which maps each of the 256 cases into an array of corresponding triangle vertices.

When the triangle mesh of the liquid's surface is being rendered, the normal vectors of the surface is needed. This project chooses to approximate the normal vector using the discrete gradient of the signed distance field, $\nabla\phi$. This vector represents the normal because, intuitively, $\nabla\phi$ points in the direction where ϕ increases the most, which is also the direction that perpendicularly points away from the liquid surface.

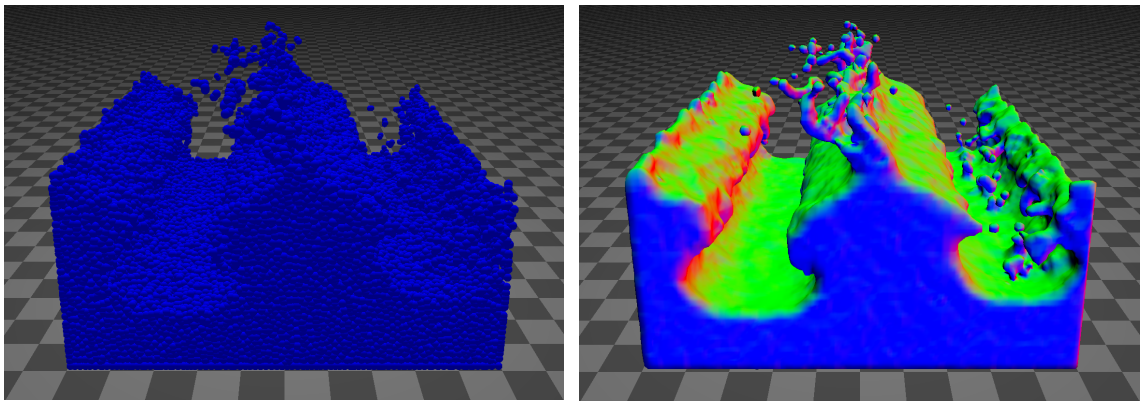

(a) Particle cloud

(b) Constructed mesh and its normal. Direction represented by colours: Red:$+x$ Green:$+y$ Blue:$+z$

Figure 5.2: Surface reconstruction from particles

5.3 Surface Shading

After the triangle mesh representing the liquid surface is constructed, it is put through the OpenGL pipeline for shading. The most important task falls upon the fragment shader, where the colour of each pixel on the mesh is computed. In order to generate realistic colouring, it is necessary to model how rays of light interact with the liquid.

5.3.1 Reflection And Refraction

As a ray of light hits the boundary between air and liquid, part of its energy is bounced away from the surface, while the rest enters the liquid and continues to travel inside. The two resulting rays are respectively called the *reflection* and the *refraction*.

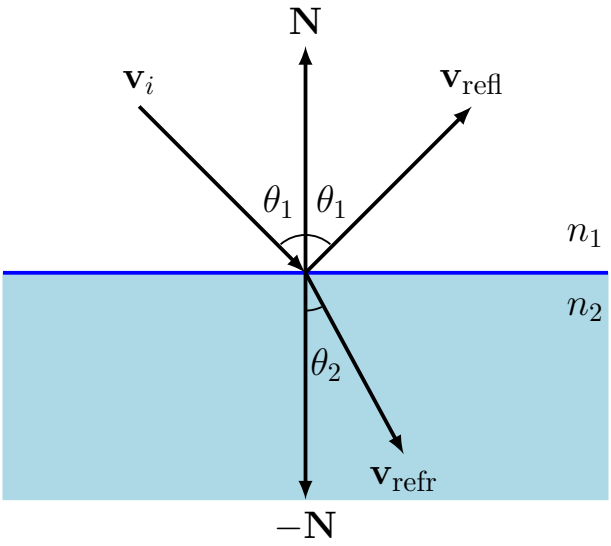

Figure 5.3: Reflection and Refraction.

Let $\mathbf{v}_i$ be the direction of the incident ray, and let $\mathbf{v}_{\text{refl}}$ be the direction of the reflected ray. The angle θ_i between $\mathbf{v}_i$ and the surface normal $\mathbf{N}$ will always be the same as the angle between $\mathbf{N}$ and $\mathbf{v}_{\text{refl}}$. Knowing $\mathbf{v}_i$ and $\mathbf{N}$, $\mathbf{v}_{\text{refl}}$ can be computed as:

$$\mathbf{v}_{\text{refl}} = 2\mathbf{N}(-\mathbf{v}_i \cdot \mathbf{N}) + \mathbf{v}_i \tag{5.2}$$

The direction of the refracted ray, $\mathbf{v}_{\text{refr}}$, is slightly more complicated to compute. The angle θ_2 between $\mathbf{v}_{\text{refr}}$ and the $-\mathbf{N}$ is governed by the Snell's law:

$$\frac{\sin\theta_1}{\sin\theta_2} = \frac{n_2}{n_1}$$

where n_1 is the *Index of Refraction* of air, and n_2 that of the liquid. Usually, n_1 is roughly equal to 1, and the n_2 for water is around 1.333. Based on Snell's law, Bec[2] derived a fast formula for computing $\mathbf{v}_{\text{refr}}$:

$$\begin{aligned} \mathbf{v}_{\text{refr}} &= (w-k)\mathbf{N} + n\mathbf{v}_i \qquad \text{where} \\ n &= \frac{n_1}{n_2} \\ w &= n(-\mathbf{v}_i \cdot \mathbf{N}) \\ k &= \sqrt{1+(m-n)(m+n)} \end{aligned} \tag{5.3}$$

Besides the direction of the reflection and refraction, it's also necessary to know the ratio of the incident energy that is reflected and refracted. Let the reflection ratio be F, then, conservation of energy dictates that the ratio of refracted energy must be $1-F$. The exact value of F is determined by the Fresnel equation, which is also dependent on the polarization and spectral distribution of the light. Due to the complexity of these equations, real-time computer graphics applications often use an approximation given by Schlick[14]:

$$\begin{aligned} F &= F_0 + (1-F_0)(1-(-\mathbf{v}_i \cdot \mathbf{N}))^5 \quad \text{,where} \\ F_0 &= \left(\frac{n_2-n_1}{n_2+n_1}\right)^2 \end{aligned} \tag{5.4}$$

In the OpenGL fragment shader, the final output colour will be F multiplied by the colour of the reflection, and $1-F$ multiplied by the colour of the refraction. The reflected colour is straightforward to compute, by tracing the ray in the direction of $\mathbf{v}_{\text{refl}}$. However, for the refracted ray, because its path lies within the liquid, it's necessary to consider the behavior of the light ray within a coloured medium. To make things more complicated, since this project supports simulating multiple phases of fluids, different fluids of different colour could be mixed together in the same region. This is explored in the next subsection.

5.3.2 Multiple Fluids Rendering

As a ray of light travels past a region of coloured liquid, the energy of the light ray diminishes as a result of scattering and absorption by the liquid particles. This process is quantified by the *Beer-Lambert Law*, which defines the ratio T_r of the light that remains after it travels through the fluid region:

$$\begin{aligned} T_r &= e^{-\tau} \quad \text{where} \\ \tau &= \int_0^d \sigma_t(\mathbf{o}+x\mathbf{v})dx \end{aligned}$$

In this formula, $\mathbf{o}$ is the point where the ray enters the liquid, $\mathbf{v}$ its direction of travel, and d the length of the path of the ray inside the water. The function $\sigma_t(\mathbf{x})$ indicates how much of the light becomes extinct at location $\mathbf{x}$, and the integral of the extinction across the entire path is τ, the *optical thickness*.

For a fluid consisting of only one type of fluid, the parameter σ_t stays constant, so τ can be computed simply as $\sigma_t d$. However, in a region where multiple fluids are mixed together, the integral must be explicitly evaluated, usually numerically.

Moreover, the extinction parameter σ_t is highly dependent on the wavelength of the light, which is precisely the cause for different fluids to have different colours. For example, a red liquid has the lowest σ_t for the wavelength of red, thereby allowing more red light to pass through. As a result, the numerical integration of τ needs to be performed for each of the RGB channels.

A frequently used method for computing τ is *ray marching*, where the ray in question is progressed a small step at a time, accumulating the extinction along the way. Alternatively, this project invented a novel algorithm for accumulating σ_t, which is more efficient and directly makes use of the FLIP particles, which carry the concentration information:

1. Create a texture image, where each colour channel (red, green, blue, alpha) in the texture will correspond to the thickness of a specific fluid phase. Note that this limits the maximum number of different fluids to 4.

2. Configure OpenGL's compositing step (see section 5.1) to perform simple addition for overlapping pixels. This means that, if a pixel is covered by more than one particles, the results from rendering those particles will be added together to form the final result. On the GPU, compositing is not computed by ALUs, but hardware accelerated by a dedicated unit called the ROP (Render Output Unit).

3. Render the FLIP particles and direct the output to the texture created in step 1. For each fluid particle p, and for each fluid phase f, render the concentration of f that p carries into the channel designated for f. The configuration from step 2 will ensure that the concentrations for all particles are accumulated.

4. While rendering the mesh, at each pixel, sample the concentration texture, and use the accumulated concentration to determine τ. The correct colouring can then be computed.

Example results of the intermediate render stages are shown in this figure:

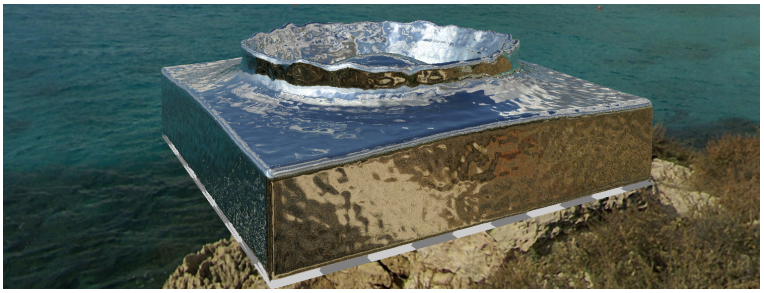

(a) The reflection

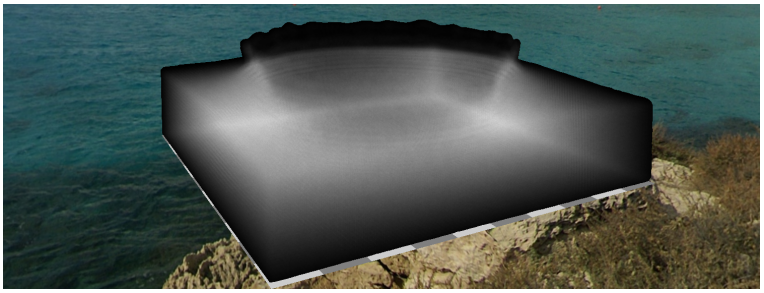

(b) The thickness texture of the blue liquid.
Brighter colour indicates greater thickness.

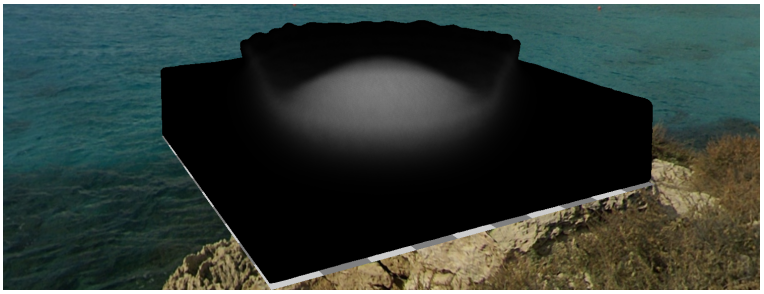

(c) The thickness texture of the red liquid

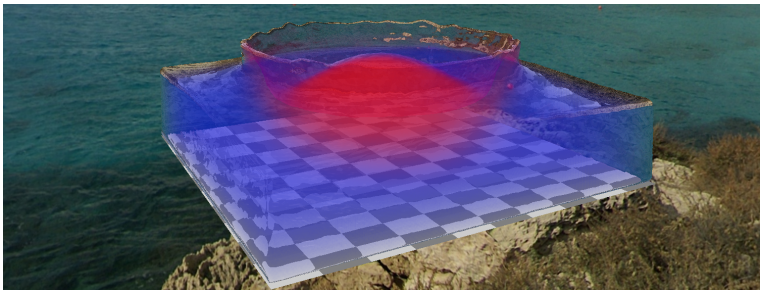

(d) The refraction colour.

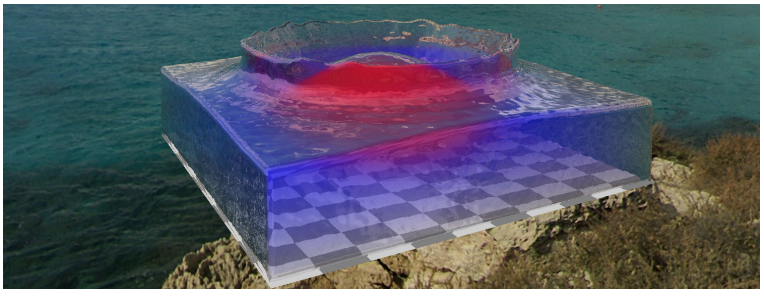

(e) Final result

Figure 5.4: Intermediary and final outputs of the renderer. The images show the moment after a large ball of red liquid falls into a box of blue liquid.

6 Results

Combining the FLIP implementation described in chapter 4 and the render algorithms in chapter 5, the software of this project is able to generate realistic images of many interesting simulations in real time. Some selected sequences of screenshots follow below.

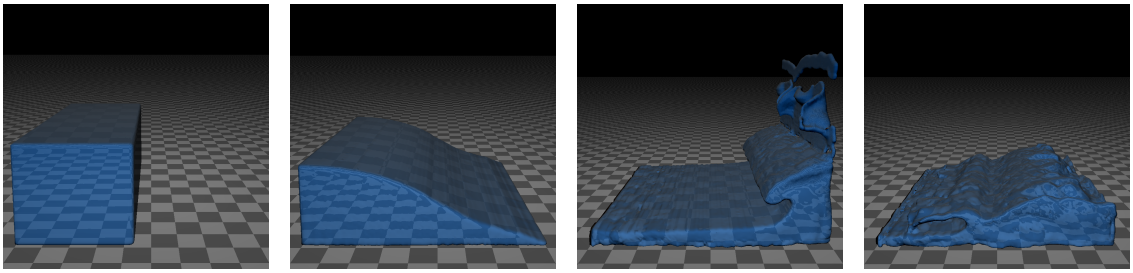

Figure 6.1: "Dam break" simulation

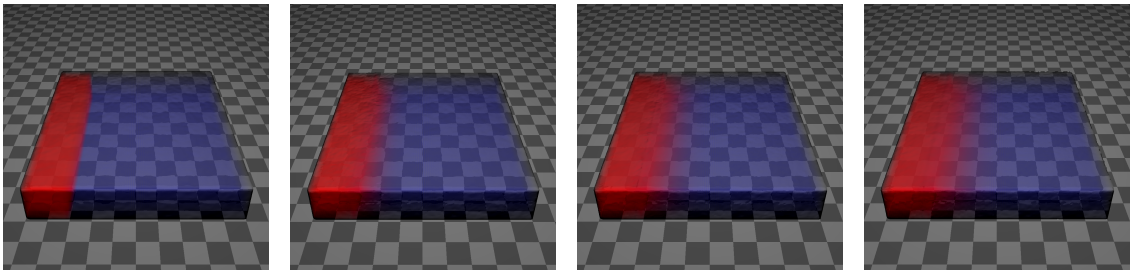

Figure 6.2: Diffusion with coefficient 10^{-3}

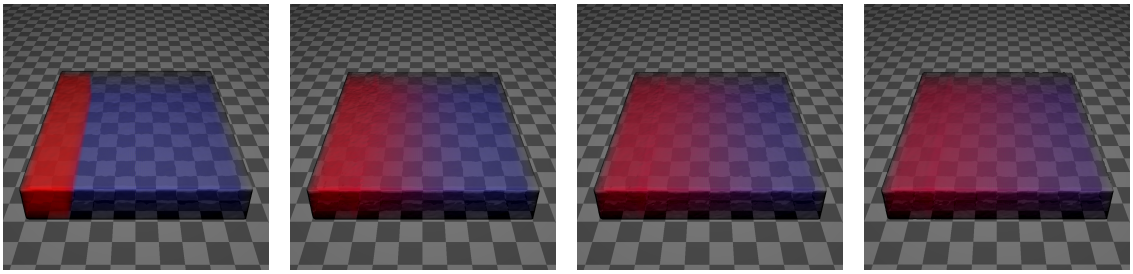

Figure 6.3: Diffusion with coefficient 10^{-2}

6.1 Performance

Performances of the software implemented in this project highly depend on the simulation parameters used. The most influential parameter is the grid resolution, which is required to be at least approximately 50^3 to give pleasing visual results. The simulation and rendering algorithms take time linear to the number of cells occupied by fluids, which is cubic to the grid resolution in each dimension. In the following figure, the empirical framerate of the software is plotted against the resolution:

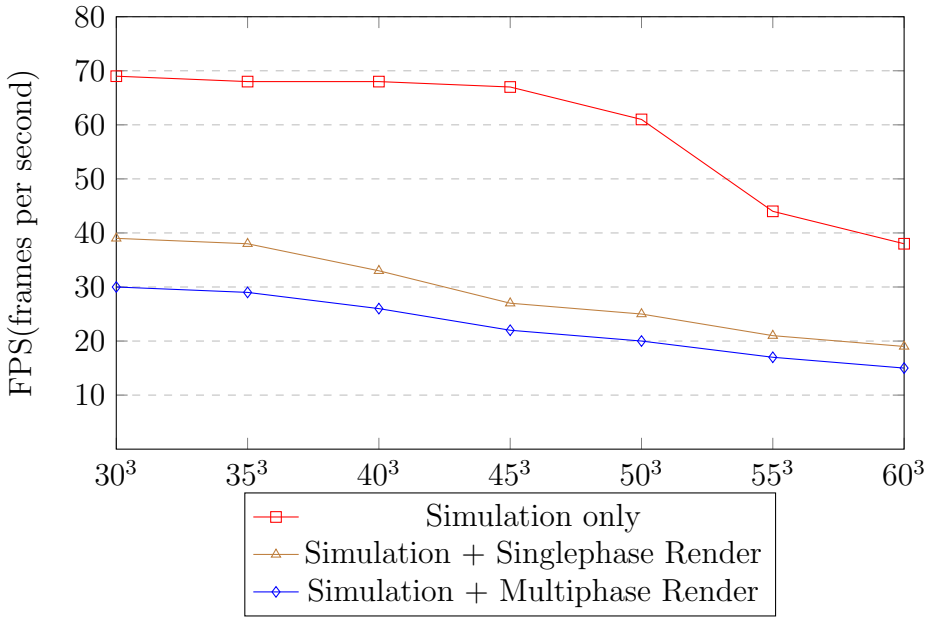

Figure 6.4: Plot of framerate against grid resolution. Each simulation uses the identical initial condition, where 25% of the domain is occupied with fluid. 100 Jacobi iterations are used in each time step. The tests are performed on a Microsoft Surface Book 2, with a i7-8650U CPU and a GTX 1060 GPU.

As a somewhat surprising observation, the computation time required to render a frame is actually considerably longer than the time taken to advance the simulation by one step. This is because, in order to generate a fine mesh, the resolution of the discrete grid of signed distance field is around 3 times the resolution of the MAC grid, which caused the surface reconstruction step (section 5.2) to be rather expensive. Furthermore, multiphase rendering is noticeably more expensive than single-phase rendering, which is because if there is only one fluid phase, the particle-based optical thickness calculation (section 5.3.2) is not required, and an approximation can be made using the tint colour of the fluid.

6.2 Comparison with Existing Software

The performance of the software created in this project is compared with a public CPU implementation of FLIP, namely the FLIP Fluids add-on[1] to Blender[2]. The same simulation parameters are used, and the programs are run on the same machine. Figure 6.5, 6.6, and 6.7 show an example comparison. In these figures, a 50^3 grid is used, which contains around $200k$ FLIP particles. While the CPU implementation in Blender takes around 1.1 seconds for each frame, the software of this project can perform simulation and rendering at 20 FPS, which is substantially faster.

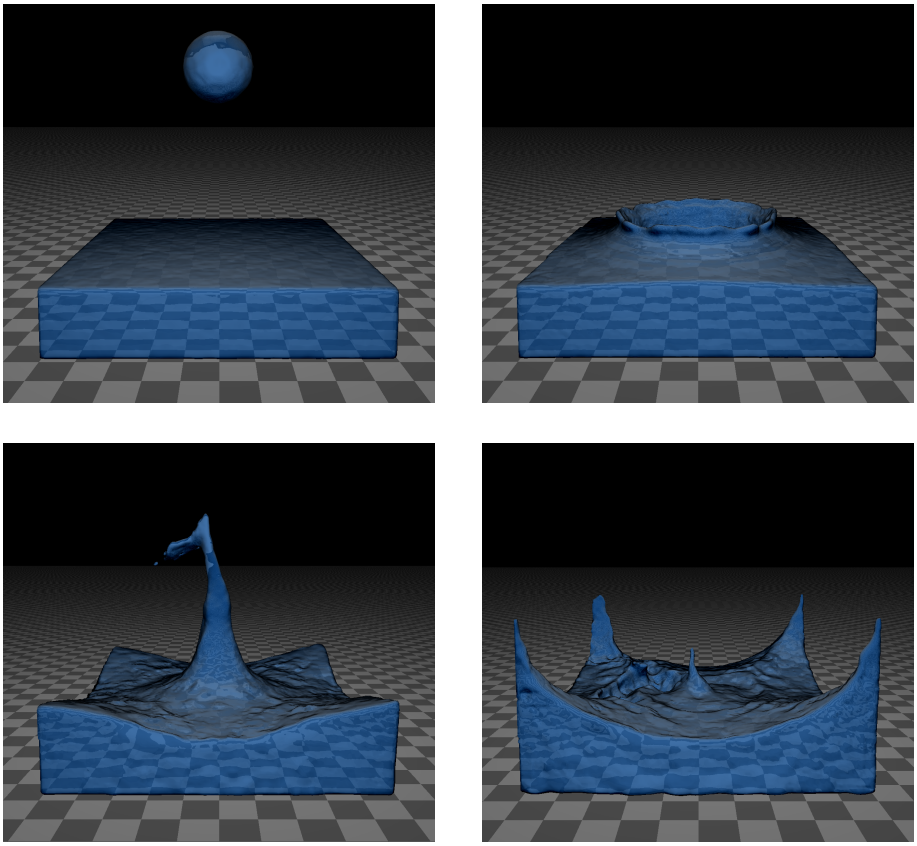

Figure 6.5: Screenshots of a "ball drop" simulation of the software created in this project.

[1] `https://blendermarket.com/products/flipfluids`
[2] `https://www.blender.org/`

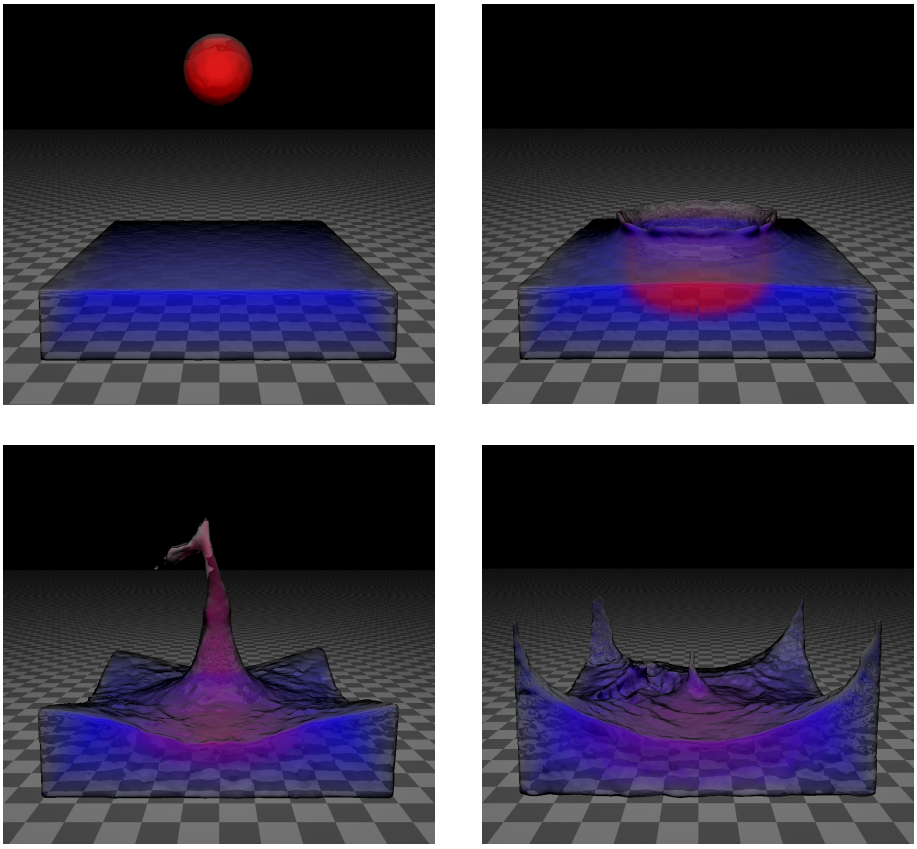

Figure 6.6: Same simulation as figure 6.5, with 2 differently coloured phases.

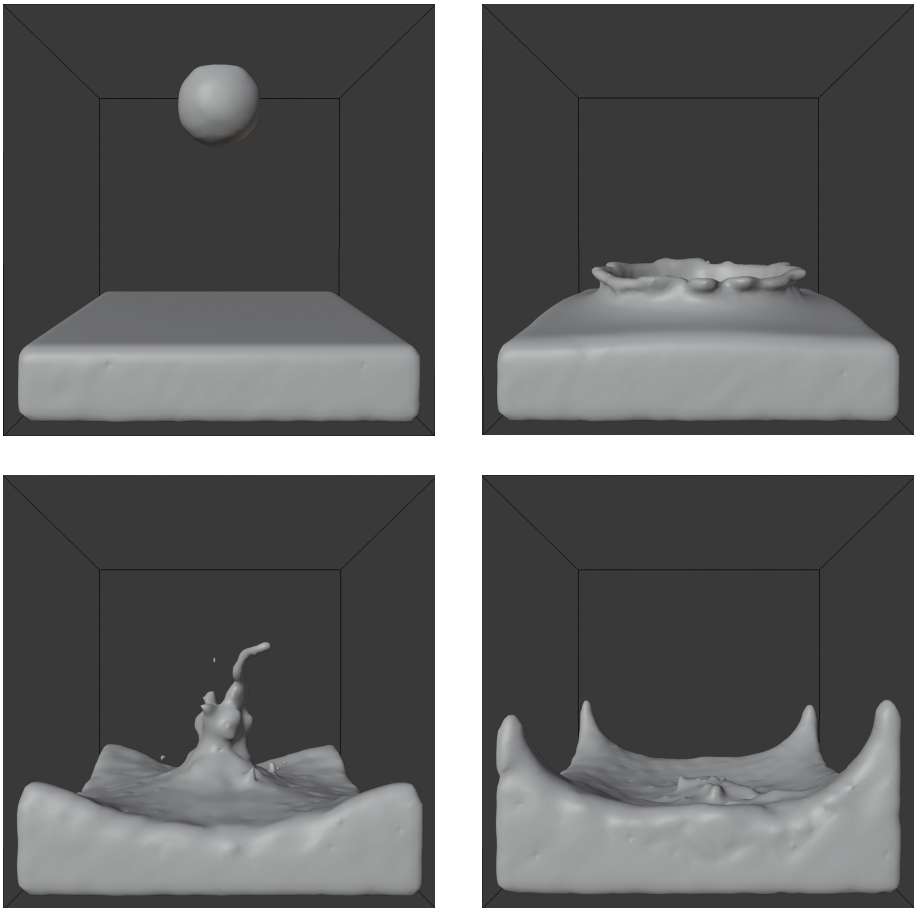

Figure 6.7: Screenshots of Blender performing the same simulation as figure 6.5.

7 Conclusions

This project explored how modern GPUs can be programmed to efficiently simulate and render multiphase fluids. A program was built that was able to perform real-time fluid simulations, and to simultaneously render and display realistic images. The project mostly focuses on parallelizing existing algorithms, but invents an original algorithm for performing fast multiphase fluid volume rendering. The software created is named *Aquarius*, and its full source code is available at `https://github.com/AmesingFlank/Aquarius`.

7.1 Limitations & Future Work

During the development of this project, many ideas emerged that would all bring more significance to this project. Unfortunately, the time permitted did not allow them to be explored. The following are a few valuable features that the program does not yet support, but could be added in future endeavors.

- Viscosity.

  This project focused on fluids that follow the Euler equations, ignoring the effect of viscosity described in the full Navier-Stokes equations. While not problematic for water-like liquids, many other interesting visual effects of fluids (e.g. melting chocolate) are only possible with viscosity.

- Solid-fluid coupling

  In the real world, the motion of fluids almost always induces or is induced by the motion of solids. Modelling the coupling between solid and fluid allows for more useful simulations.

- Caustics, shadows, and foams

  The renderer built in this project is far from complete, as there are still a lot of optical features not captured. The curved shapes of liquids can cause

the refracted light to be focused onto certain areas, creating an alternating pattern of brightness and darkness, known as caustics and shadows. Also, fast-moving liquids sometimes have small regions that trap volumes of air, creating foams. These phenomenons are common in real life, and supporting them in the renderer can significantly increase the realism of the images generated.

- Publishing as a library

  In its current form, the software created by this project has limited practical use. However, with some extra engineering, the code could be turned into a distributable library that can be used to perform fluid simulation in other projects. Specifically, it could be adapted into a plugin for popular game engines such as Unity or Unreal, so that game programmers can use it to easily incorporate real-time fluids in their work.

7.2 Personal Reflections

Working on this project has been a gratifying experience. The topic is fascinating, and there was so much I learnt during the process. Apart from the improvements mentioned in 7.1, which I wish I could have made more progress in, I am in general very happy with and proud of the results I achieved.

When I submitted the proposal of this project in February 2019, it was purely based on interest as I had no previous experience and understanding of fluid simulation. So, the first thing I had to do in this project was to learn about the physics of fluids. As a pure computer science student, this proved challenging, because the mathematics courses that CS students take do not cover much vector calculus. In the Easter vacation of 2019, I spent a substantial amount of time catching up with vector calculus and fluid dynamics, which was difficult, but layed the ground for my future efforts.

Before I started reading academic papers on the topic, I read a book called *Fluid Simulation for Computer Graphics*[3], written by Robert Bridson, one of the leading experts in the field. This book gave a piece of really good advice: always start by writing a 2D simulator, before moving on to 3D. I did follow this advice, and took it one step further: I started by writing code that only runs on CPU, before moving on to a GPU implementation. This was definitely a good idea because, considering the level of complexity of my GPU implementation right now, it would have been impossible for me to implement it correctly when I was still very unfamiliar with the

problem at hand. A lesson learnt here is that for complicated tasks, a good way to start is by building a simple prototype.

One of the biggest challenges that I faced in this project is the performance of my program. When I first ported my CPU 2D fluid simulator code to GPU, the simulation was only running at an embarrassing 7 frames per second, without even incorporating any sophisticated rendering. I was quite anxious about this, because I really wished to achieve real-time simulation and rendering, and that is for 3D. At that time, the performance problem was caused by the pressure solver (section 3.5), which was taking tremendously long to solve the pressure Poisson equation. After weeks of careful analysis, a few optimization tricks, and some helpful directions pointed out by my supervisor, Dr. Joe Pitt-Francis, I eventually resolved this issue. There isn't a specific moral in overcoming this obstacle, but I certainly learnt a lot about numerical computation and GPU optimization because of it.

I absolutely enjoyed learning about fluids and coding a simulator, but, somewhat surprisingly, I also enjoyed writing this report very much. Not only was I able to talk about a project that I worked passionately on, but as I reiterated the methods I used, I cleared up a few technical details which I did not completely understand. Although, I found it quite stressful to obey the 10,000-word limit. There are a few mathematical details and some experimental methods (e.g. PBF and PCISPH), which I spent a considerable amount of time working on, but sadly could not fit into this report.

This project is possibly the most significant intellectual endeavor I have made in my years at Oxford (though waiting to be surpassed by my 4th-year project), and I find it to be an unmissable part of my education. Through this project, I was exposed to many spectacular areas of computer graphics that I did not know existed, and I was familiarized with the techniques essential to these studies. I have grown as a computer science student because of this project.

Bibliography

[1] Alexis Angelidis and Fabrice Neyret. Simulation of smoke based on vortex filament primitives. In *Proceedings of the 2005 ACM SIGGRAPH/Eurographics symposium on Computer animation*, pages 87–96, 2005.

[2] Xavier Bec. Faster refraction formula and transmission color filtering. *Ray Tracing News*, 10(1):396, 1997.

[3] Robert Bridson. *Fluid simulation for computer graphics*. CRC press, 2015.

[4] Nuttapong Chentanez and Matthias Müller. Real-time eulerian water simulation using a restricted tall cell grid. In *ACM Siggraph 2011 Papers*, pages 1–10. 2011.

[5] Simon Green. Cuda particles. *NVIDIA whitepaper*, 2(3.2):1, 2008.

[6] Francis H Harlow and J Eddie Welch. Numerical calculation of time-dependent viscous incompressible flow of fluid with free surface. *The physics of fluids*, 8(12):2182–2189, 1965.

[7] Nahyup Kang, Jinho Park, Junyong Noh, and Sung Yong Shin. A hybrid approach to multiple fluid simulation using volume fractions. In *Computer Graphics Forum*, volume 29, pages 685–694. Wiley Online Library, 2010.

[8] ByungMoon Kim, Yingjie Liu, Ignacio Llamas, and Jaroslaw R Rossignac. Flowfixer: Using bfecc for fluid simulation. Technical report, Georgia Institute of Technology, 2005.

[9] William E Lorensen and Harvey E Cline. Marching cubes: A high resolution 3d surface construction algorithm. *ACM siggraph computer graphics*, 21(4):163–169, 1987.

[10] Leon B Lucy. A numerical approach to the testing of the fission hypothesis. *The astronomical journal*, 82:1013–1024, 1977.

[11] Miles Macklin and Matthias Müller. Position based fluids. *ACM Transactions on Graphics (TOG)*, 32(4):1–12, 2013.

[12] Joe J Monaghan. Smoothed particle hydrodynamics. *Annual review of astronomy and astrophysics*, 30(1):543–574, 1992.

[13] Matthias Müller, David Charypar, and Markus Gross. Particle-based fluid simulation for interactive applications. In *Proceedings of the 2003 ACM SIGGRAPH/Eurographics symposium on Computer animation*, pages 154–159. Eurographics Association, 2003.

[14] Christophe Schlick. An inexpensive brdf model for physically-based rendering. In *Computer graphics forum*, volume 13, pages 233–246. Wiley Online Library, 1994.

[15] Andrew Selle, Ronald Fedkiw, Byungmoon Kim, Yingjie Liu, and Jarek Rossignac. An unconditionally stable maccormack method. *Journal of Scientific Computing*, 35(2-3):350–371, 2008.

[16] Barbara Solenthaler and Renato Pajarola. Predictive-corrective incompressible sph. In *ACM SIGGRAPH 2009 papers*, pages 1–6. 2009.

[17] Wladimir J van der Laan, Simon Green, and Miguel Sainz. Screen space fluid rendering with curvature flow. In *Proceedings of the 2009 symposium on Interactive 3D graphics and games*, pages 91–98, 2009.

[18] Geoff Wyvill, Craig McPheeters, and Brian Wyvill. Soft objects. In *Advanced Computer Graphics*, pages 113–128. Springer, 1986.

[19] Shibiao Xu, Xing Mei, Weiming Dong, Zhiyi Zhang, and Xiaopeng Zhang. Interactive visual simulation of dynamic ink diffusion effects. In *Proceedings of the 10th International Conference on Virtual Reality Continuum and Its Applications in Industry*, pages 109–116, 2011.

[20] Yongning Zhu and Robert Bridson. Animating sand as a fluid. *ACM Transactions on Graphics (TOG)*, 24(3):965–972, 2005.